



# A global map of Local Climate Zones to support earth system modelling and urban scale environmental science

Matthias Demuzere<sup>1</sup>, Jonas Kittner<sup>1</sup>, Alberto Martilli<sup>2</sup>, Gerald Mills<sup>3</sup>, Christian Moede<sup>1</sup>, Iain D. Stewart<sup>4</sup>, Jasper van Vliet<sup>5</sup>, and Benjamin Bechtel<sup>1</sup>

<sup>1</sup>Urban Climatology Group, Department of Geography, Ruhr-University Bochum, Bochum, Germany

<sup>2</sup>Environmental Department, CIEMAT, Spain

<sup>3</sup>School of Geography, University College Dublin, Dublin, Ireland

<sup>4</sup>Global Cities Institute, University of Toronto, Toronto, Ontario, Canada

<sup>5</sup>Institute for Environmental Studies, Vrije Universiteit Amsterdam, De Boelelaan 1085, 1081, HV, Amsterdam, the Netherlands

**Correspondence:** Matthias Demuzere (matthias.demuzere@rub.de)

**Abstract.** There is a scientific consensus on the need for spatially detailed information on urban landscapes at a global scale. This data can support a range of environmental services, as cities are acknowledged as places of intense resource consumption and waste generation and foci of population and infrastructure that are exposed to multiple hazards of natural and anthropogenic origin. In the face of climate change, urban data is also required to explore future urbanisation pathways and urban design strategies, in order to lock in long-term resilience and sustainability, protecting cities from future decisions that could undermine their adaptability. To serve this purpose, we present a 100m resolution global map of Local Climate Zones (LCZs), an universal urban typology that can distinguish urban areas on a holistic basis, accounting for the typical combination of micro-scale land-covers and associated physical properties. The global LCZ map, composed of 10 built and 7 natural land cover types, is generated by feeding an unprecedented amount of labelled training areas and earth observation imagery into lightweight random forest models. Its quality is assessed using a bootstrap cross validation alongside a thematic benchmark for 150 selected functional urban areas using independent global and open-source data on surface cover, surface imperviousness, building height, and anthropogenic heat. As each LCZ type is associated with generic numerical descriptions of key urban canopy parameters that regulate atmospheric responses to urbanisation, the availability of this globally consistent and climate-relevant urban description is an important prerequisite for supporting model development and creating evidence-based climate-sensitive urban planning policies. This dataset can be downloaded from <http://doi.org/10.5281/zenodo.6364594> (Demuzere et al., 2022a).

## 1 Introduction

Cities are at the forefront of global climate change science owing to their emissions of greenhouse gases and their exposure to the projected hazards, such as sea-level rise and warming (IPCC, 2022). As a result, they are focus for mitigation and adaptation policies and, as they have governance structures in place, are an ideal scale to affect change. The crucial role that cities can play in this arena is recognised at the international level: the new United Nations Agenda and the 11<sup>th</sup> Sustainable Development



Goal focus on urban resilience, climate and environment sustainability of cities; two of the four challenges identified by the World Meteorological Organisation (WMO) World Weather Research Program are urban related: high-impact weather, including impacts in cities, and urbanisation; the Intergovernmental Panel on Climate Change Cities and Climate Change Scientific Committee identified six research priorities for science to have a stronger role in urban policy and practice; and advocacy groups like C40<sup>1</sup> play an increasingly important role in achieving national emission targets and enhancing resilience (Creutzig et al., 2016; Bai et al., 2018; Masson et al., 2020).

Cities are simultaneously drivers of regional and local climate changes. The conversion of Earth's land surface to urban areas is one of the most irreversible human impacts on the global ecosystem (Grimm et al., 2008; Reba and Seto, 2020). In addition to the many modifications to bio-, hydro-, and lithosphere (Seto et al., 2012; D'Amour et al., 2017; Liu et al., 2019; van Vliet, 2019; Zhang et al., 2019; McDonough et al., 2020), urbanisation affects energy demand (Creutzig et al., 2015; Güneralp et al., 2017), releases anthropogenic heat emissions and pollutants (Patella et al., 2018; Takane et al., 2019), and alters the urban climate (Oke et al., 2017). Current and future climate changes represent significant risks to urban populations and to the natural and physical infrastructure systems of cities (Costello et al., 2009; UN, 2019; Wang et al., 2021). In this context, the WMO has advocated the development on integrated urban services (IUS) – using observations (remote and in situ) and models - that addresses the panoply of hazards that cities face and the needs of service providers, including emergency services, public health bodies, energy produces, urban designers and planners, etc. (Baklanov et al., 2018; Grimmond et al., 2020).

Despite their importance as a spatial nexus of climate drivers and of governance, cities are largely excluded from global climate science owing to their relatively small extent and our limited knowledge of their spatial structures. Earth System Models (ESMs) have only recently evolved to accommodate urban-scale landscapes, even though the parameters that are used by ESMs to these landscapes are limited in scope. At regional and urban scales, model developments use far more detailed parameters that include descriptions of the net impacts of buildings in creating a distinct urban canopy and boundary layers. While some theoretical challenges remain, it is now possible to simulate urban effects on climate, between and above buildings at sub-urban scales (Barlow, 2014). Scientific advances will soon allow variable scale modelling that will incorporate the hierarchy of climate processes and impacts. However, the absence of suitable and universal global urban landscape data to inform these models represents a serious impediment to progress (Zhao et al., 2021; Hertwig et al., 2021). What is needed is a comprehensive database on cities globally that supports multi-scale modelling, provides a spatial framework for interpreting on-site and remote measurements and allows the meaningful transfer of knowledge among and within cities (Rosenzweig et al., 2010; Hidalgo et al., 2018).

The critical data needed to support urban climate science includes information on urban form and functions. Measures of form include building density, street widths, building heights, construction materials and fraction of vegetated areas. These attributes largely influences the local climate and the 'adaptation' capacity of a city (e. g. to ensure a comfortable thermal

<sup>1</sup><https://www.c40.org/cop26/>



environment to its inhabitants). Urban functions describe the emissions of waste heat, materials and gases into the overlying atmosphere. Appropriate measures would include the anthropogenic heat flux (AHF) and CO<sub>2</sub> emissions. Form and function are correlated, for example: population density regulates energy consumption, and therefore the potential to mitigate global warming by reducing the greenhouse gas emissions; variations in building layout and heights moderates surface roughness and contributes to the atmospheric dispersive conditions, and so the air quality (Martilli, 2014). Models are needed to assess the net benefits of climate-based interventions that may have unintended outcomes. For example, densely built and occupied cities (so called compact 15-minute cities) will reduce traffic, energy demand and CO<sub>2</sub> emissions, and in some cases improve air quality (Stone et al., 2007; McDonough et al., 2020; Williams et al., 2010), but will enhance warming and heat stress by reducing vegetative cover and sky view factor in the street canyons, and increase the spatial density of the anthropogenic heat (Demuzere et al., 2014; Lai et al., 2019). Understanding how different urban forms interact with the atmosphere is key to redesigning cities, and, more importantly, plan future urbanisation. It is therefore essential to have information that differentiates between urban forms that can be used by atmospheric models to simulate the future climatic conditions and different urban form scenarios. Our objective here is to generate these data to support model evolution and stimulate research on multi-scale climate projections to manage urban risks.

70

Acquiring urban data at a global scale is not a trivial exercise owing to the operational definition of ‘urban’, the scattered extents of cities globally and their complex intra-urban geographies; for example, the Global Human Settlement Layer Urban Centres Database identifies over 13.000 settlements (Florczyk et al., 2019), while Li et al. (2020b) generated over 60.000 global urban boundaries. At the global scale, there are several datasets that identify the extent of contiguous urban areas, based on built-up or impervious surface cover (Zhou et al., 2015; Corbane et al., 2017; Esch et al., 2017; Marconcini et al., 2020; Gong et al., 2020; Zhang et al., 2020a; Zhao et al., 2022) but none that provide intra-urban morphological details (green cover, built density, building heights, etc.) that are needed by scientists to generate the urban canopy parameters (UCPs) to run models and by urban policy-makers to make informed decisions based on analyses of risk. For many cities, relevant information may be gleaned from local sources that maintain municipal geographic databases (e.g. Biljecki et al., 2021), but these data vary in terms of their quality, consistency, and accessibility, which limits their wider applicability (Zhu et al., 2019). The 100 m resolution global Local Climate Zone (LCZ) map presented here addresses this need for more detailed intra-urban data. This product is the outcome of more than a decade of research on how best to acquire, evaluate and deploy urban data in support of climate science (Stewart and Oke, 2012; Bechtel and Daneke, 2012; Ching et al., 2018).

85 The LCZ typology is currently the only universal classification that categorises urban landscapes using a scheme that identifies readily recognisable neighbourhood types based on their form and function, which modify the surface energy and water budgets. Critically, each LCZ type is linked to meaningful UCP value ranges that can be used for physically-based modelling (Stewart and Oke, 2012; Ching et al., 2019; Demuzere et al., 2020a). It goes beyond the urban mask and enables the assessment of the spatial impact of urban planning decisions that will alter UCPs and their climate outcomes. The LCZ scheme is distinguished from other LULC schemes by its focus on urban and rural landscape types, which can be described by any of the 17

90



classes in the scheme (Fig. 1). The scheme was originally designed to encourage climate change researchers to step away from their computers and get acquainted with the field sites that support their work, to capture the character of the urban landscape responsible for the urban heat island (UHI), and to ensure consistent reporting of metadata about the sites used to measure the heat island effect (Stewart, 2018; Stewart and Mills, 2021). The World Urban Database and Access Portal Tools (WUDAPT) project has adopted the scheme in pursuit of its goal ‘to capture consistent information on cities worldwide that can support urban weather, climate, hydrology and air quality modelling’ Ching et al. (2018). The global LCZ product for the first time captures the intra-urban heterogeneity across the whole surface of the Earth, capturing cities of all sizes. It complements the LCZ maps for individual cities created by the WUDAPT community, the LCZ Generator <sup>2</sup> (Demuzere et al., 2021b) or that are available via other sources (e.g. Taubenböck et al., 2020; Zhu et al., 2022). In addition, as each LCZ type is associated with generic numerical descriptions of key UCPs, the availability of this globally consistent and climate-relevant urban description is an important prerequisite to advance our capacity to assess climate risks at urban scales, and enable the development of fit-for-purpose climate mitigation and adaptation strategies.

---

<sup>2</sup><https://lcz-generator.rub.de/>



**Figure 1.** Definitions of built (1-10) and land cover types (A-G) for the Local Climate Zone scheme (Stewart and Oke, 2012; Demuzere et al., 2020a).



## 2 Methods and Data

105 Whilst many LCZ mapping methodologies are currently available (see e.g. review by Jiang et al., 2021), the methodology for the global LCZ map follows WUDAPT's default protocol that was launched by (Bechtel et al., 2015), sequentially improved by Demuzere et al. (2019b, a, 2020a), ultimately leading to the LCZ Generator (Demuzere et al., 2021b), a web application that makes single-city LCZ mapping fast and easy. The procedure requires labelled training areas, earth observation input data, and a random forest model, discussed in-depth in Sections 2.1, 2.2 and 2.3 respectively. In addition, in line with previous continental-scale LCZ mapping efforts by Demuzere et al. (2019b, 2020a), the quality of the resulting LCZ map is assessed in  
110 two ways: 1) a traditional quality assessment using multiple accuracy metrics, and 2) a thematic benchmark, by translating the LCZ map into its corresponding LCZ-based urban canopy parameters, and comparing these against (semi-)independent global and open-source databases reflecting urban forms and functions (Section 2.4).

### 2.1 Training areas

115 Training areas (TAs) are LCZ-labelled polygons that represent typical examples of built or natural LCZs in a region of interest (ROI). By design, they are compiled in a crowd-sourced manner, either by urban experts (Bechtel et al., 2015) or alternative crowd-sourcing platforms such as MTurk (<https://www.mturk.com>) (Demuzere et al., 2020a; Xu et al., 2021) using good practice guidelines for digitising TAs (see Appendix A and Demuzere et al. (2021b)). While the LCZ maps created by individuals are often of poor to moderate quality, The Human Influence Experiment (HUMINEX) (Bechtel et al., 2017; Verdonck et al., 2019a) demonstrated large accuracy improvements (up to 20%) when multiple (poor to moderate quality) training datasets were  
120 used together to create a single LCZ map. In the current study, TAs are compiled from multiple sources. First, well-trained students assistants from the Ruhr-University Bochum produced TA sets for more than 100 global ROIs (labelled as RUB). Second, archived TA (labelled as ARC) sets were collected from previous published research and collaborations, including the samples hosted on the old WUDAPT portal (<https://www.wudapt.org/the-wudapt-portal/>). Finally, the RUB and ARC TA sets are supplemented with the TA samples available from the LCZ Generator (Demuzere et al., 2021b) (labelled as GEN).

125

Before being used in the classification procedure, all TA sets are curated. First, all RUB and ARC training area sets are submitted to the LCZ Generator: in case of multiple entries for one submission, only the best submission is retained. Also, only TA samples mapped to LCZs with an overall accuracy greater than 50% are kept. Second, in case of duplicate regions across the different sources, the following priority is used: RUB > ARC > GEN. Third, only the original seventeen LCZ  
130 classes are kept, thereby removing non-standardized classes available in some of the samples, such as LCZ W - Wetlands (Brousse et al., 2019, 2020b, a) and LCZ H - Agricultural greenhouses (Vandamme et al., 2019). Third, in order to maintain computational efficiency, and to avoid redundancy and mixed spectral characteristics, the surface area of large polygons (>1.5 km<sup>2</sup>) is reduced, and too small or too complex TA polygons are removed (Demuzere et al., 2021b). Finally, all pixels embedded within the ROIs are assigned to urban ecoregions (ER), which are regional clusters based on climate, vegetation, and urban



135 topology (Schneider et al., 2010)). This is based on the finding of Demuzere et al. (2019b) that ERs can provide a basis for  
intelligent learning between cities and allow upscaling from individual cities to regional and global levels.

## 2.2 Earth observation input data

In addition to the TAs, one needs earth observation (EO) input data to feed the LCZ supervised random forest classifier (Breiman, 2001; Bechtel et al., 2015). The 33 global earth observation input features used by default in the LCZ Generator (see  
140 Table 2 in Demuzere et al., 2021b) serve as a baseline. However, some EO input features are updated or added. The original  
1 km global forest canopy height representative for 2005 (Simard et al., 2011) is replaced by the 30 m global forest canopy  
height dataset representative for 2019, developed by Potapov et al. (2021) through the integration of the Global Ecosystem  
Dynamics Investigation (GEDI) lidar instrument data (April–October 2019) and multi-temporal metrics derived from Landsat.  
Also the ALOS Digital Surface Model (DSM) data is updated to version 3.2, an improved version that reconsiders the format  
145 in the high latitude area, auxiliary data, and processing method (Tadono et al., 2016). In addition, the SRTM Digital Elevation  
Model (DEM) information is replaced by the MERIT DEM (Multi-Error-Removed Improved-Terrain Digital Elevation  
Model, Yamazaki et al. (2017)), from which also the slope and aspect are added. Because of the changes in the DSM and  
DEM, also the Canopy Height Model CHM (=DSM-DEM) data is updated. Building further upon the findings of Brousse et al.  
(2020a), Hay Chung et al. (2021) and Chen et al. (2021a), two more sets of input features are added, including: 1) Gray Level  
150 Co-occurrence Matrix (GLCM) texture features (contrast, dissimilarity, inertia, sum average, and cluster shade) derived from  
PALSAR (Phased Array type L-band Synthetic Aperture Radar) for both HH and HV polarisations with a 4 by 4 kernel size  
(matching the LCZ 100 m spatial resolution), and 2) NANTLI, a Landsat 8 NDVI-adjusted (Normalized Difference Vegeta-  
tion Index) Night-Time Light Index based on VIIRS (Visible Infrared Imaging Radiometer Suite) data, analogous to EANTLI  
(Zhuo et al., 2015, 2018; Zhang et al., 2020a). See Appendix B for more details on these additional input features. Combined,  
155 this results in a set of 46 earth observation input features, derived from Landsat 8 (16), Sentinel-1 (5), Sentinel-2 (8), PALSAR  
(10), VIIRS (1) and other sources (6).

## 2.3 Lightweight global random forest models

To date, the pixel-based LCZ mapping methods have used a wide variety of machine learning algorithms to classify LCZs (see  
160 e.g. Section 3.1.4 in Jiang et al. (2021) for more details). Here, WUDAPT's initial and default (Bechtel et al., 2015) random  
forest classifier algorithm is used, building further upon the classification procedure of the LCZ Generator (Demuzere et al.,  
2021b), that uses Breiman's random forest implementation in Google's Earth Engine (EE), in combination with an automated  
cross-validation approach using 25 bootstraps (Breiman, 2001; Bechtel et al., 2015; Gorelick et al., 2017; Demuzere et al.,  
2019a, 2020a, 2021b). Yet given the sheer size of the classification problem (2+ million labels and 46 input features), two se-  
165 quential pathways (Figure 2) are developed that lead to lightweight global random forest models that balance optimal learning  
with accuracy, computational feasibility and efficiency (Corbane et al., 2021).

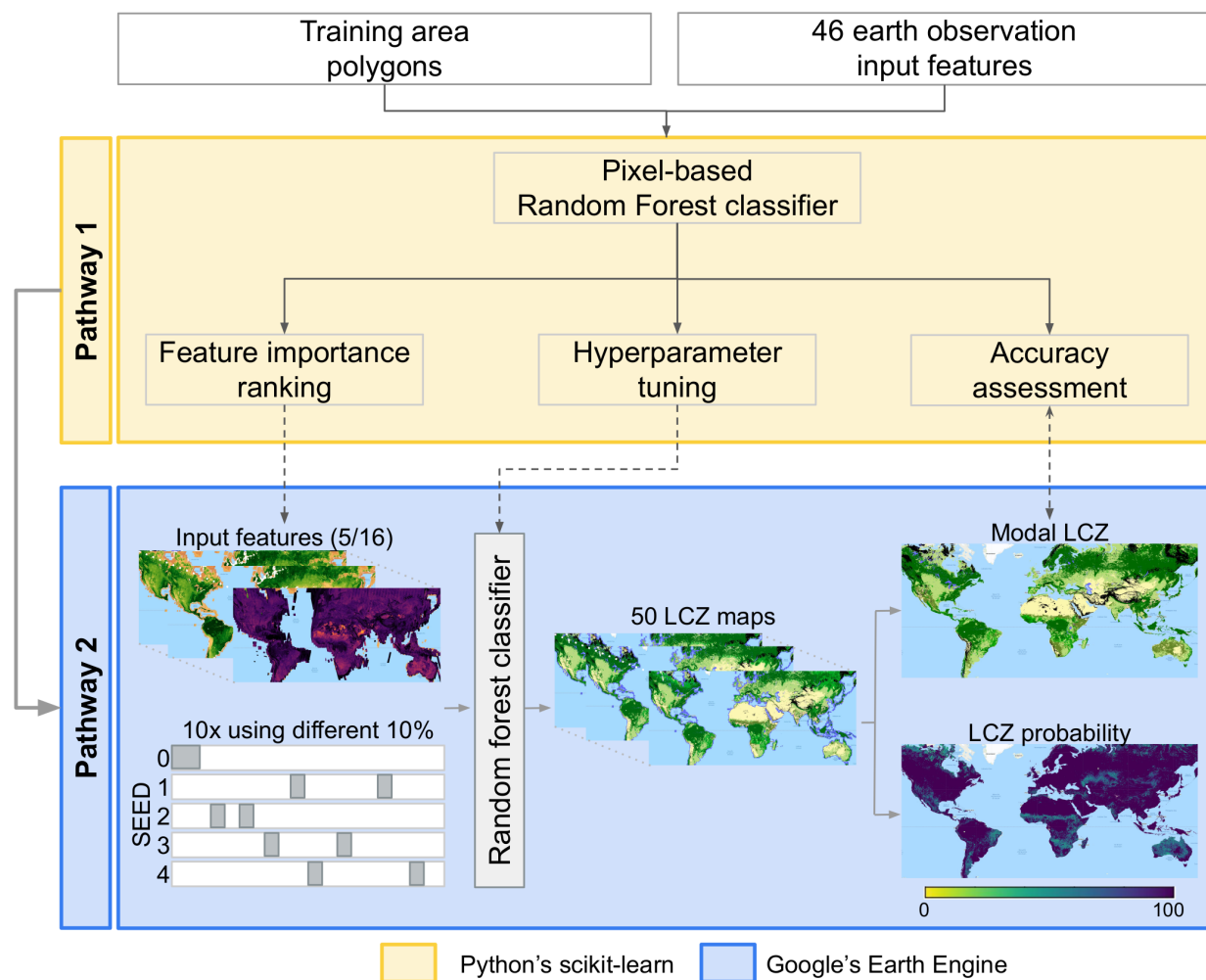


**Figure 2.** Schematic representation of the sequential pathways to develop the global LCZ map.

In a first pathway, earth observation data are extracted from all input features and for all pixels embedded within the training area polygons. Then, using Python’s random forest from the scikit-learn 0.24.2 package (Pedregosa et al., 2011) and the RF parameters used in previous work by Demuzere et al. (2019a, 2020a, 2021b), a feature importance ranking is performed (Demuzere et al., 2019b, a), for the global TA set and 15 distinct TA sets stratified by urban ecoregion. Simultaneously, the quality of these random forest classifications are assessed (see Section 2.4 for more information) by bootstrapping the classification 25 times, for the global TA set and the 15 urban ecoregions, each time using a stratified (LCZ class) random TA sampling of 70 / 30% for training / testing. In addition, a hyperparameter tuning on EE’s random forest parameters (e.g. number of trees, maximum number of leaf nodes in each tree, minimum leaf population) was applied using Python’s RandomSearchCV and GridSearchCV (Pedregosa et al., 2011) packages (not shown). But as the effect of different random forest parameters on the



overall accuracy was insignificant, the default random forest parameters were kept in pathway two.

The second pathway ingests the results from the first pathway to develop multiple lightweight global random forest models within EE. First, the final input feature set is composed of the input features that belong at least 5 times (out of 16, reflecting the global and 15 urban ecoregions) to the top 50% of most important features, obtained in pathway 1. Second, TA polygons are sampled in a double cross-folding manner, using 5 seeds (random samples) and 10% of the resulting TA samples. This is repeated 10 times, each time extracting a different 10% from the corresponding seed, resulting in 50 LCZ labels per pixel. Note that this random sampling is balanced across LCZ labels and urban ecoregions, a sampling approach that meets the three criteria as outlined by (Corbane et al., 2021; Xu et al., 2021): class balance, diversity, and representativeness. In a final step, the modal LCZ class is selected as the final LCZ label, and the resulting global modal LCZ map is post-processed using the morphological Gaussian filter described in (Demuzere et al., 2020a, 2021b). In addition, a probability layer is produced that identifies how often the modal LCZ was chosen per pixel (e.g. a probability of 60% means that the modal LCZ class was mapped 30 times out of 50 LCZ models).

## 190 2.4 Quality assessment and benchmarking

### 2.4.1 Traditional quality assessment

In order to assess the quality of the global LCZ map, the accuracy assessment from pathway 1 is repeated using the selected earth observation features only. Also here, the pixel-based random forest classification is repeated 50 times (5 seeds  $\times$  10 distinct TA samples), and for each iteration, the TA sample is randomly split in a balanced manner (by urban ecoregion and LCZ class) using 70 / 30% for training / testing. In order to avoid spatial autocorrelation that can lead to inflated accuracies, the ‘splitting the polygon pool’ approach is used (Xu et al., 2021), in which the polygons (rather than the individual pixels) are randomly sampled into 70/30 training / testing groups. The quality assessment is done using a range of well-accepted LCZ accuracy metrics, including: overall accuracy (OA), overall accuracy for the urban LCZ classes only ( $OA_u$ ), overall accuracy of the built versus natural LCZ classes only ( $OA_{bu}$ ), a weighted accuracy ( $OA_w$ ), and the class-wise metric F1 (Chinchor, 1992; Bechtel et al., 2017; Verdonck et al., 2017; Demuzere et al., 2019b, a; Bechtel et al., 2020). The overall accuracy denotes the percentage of correctly classified pixels.  $OA_u$  reflects the percentage of correctly classified pixels from the urban LCZ classes only, and  $OA_{bu}$  is the overall accuracy of the built versus natural LCZ classes only, ignoring their internal differentiation. The weighted accuracy ( $OA_w$ ) is obtained by applying weights to the confusion matrix and accounts for the (dis)similarity between LCZ types (Bechtel et al., 2017, 2020). As such, confusion between dissimilar types (e.g. LCZs 1 A) is penalised more than confusion between similar classes (e.g. LCZs 1 and 2). Finally, the class-wise accuracy is evaluated using the F1 metric, which is a harmonic mean of the user’s and producer’s accuracy (Chinchor, 1992; Verdonck et al., 2017).



## 2.4.2 Thematic benchmark

A drawback of the traditional accuracy assessment is that only pixels within TA polygons are evaluated, and those outside are not quality-controlled. In addition, high overall accuracies do not automatically mean that the resulting LCZ map is correct, as e.g. an insufficient discrimination of LCZ types in the training sample can lead to an artificially high OA. To accommodate such limitations, the resulting LCZ map can be converted to its corresponding urban canopy parameters (Table 1), that are key in urban ecosystem processes (Stewart and Oke, 2012; Oke et al., 2017; Ching et al., 2018, 2019), and that offer an indirect thematic evaluation of the mapped LCZ quality. These UCP value ranges are not site-specific, but are designed to be universally applicable to all cities, since they are based on data gathered from a large sample of measurement studies, modelling studies, existing land-cover classifications, and urban climate literature reviews (Stewart, 2011a; Stewart and Oke, 2012). And even though this strategy gives rise to other limitations and challenges (e.g. having only indirect observations available, or bumping into spatial and temporal resolution mismatches), it does however reveal the holistic nature of the LCZ typology that distinguish urban surfaces accounting for their typical combination of micro-scale land-covers and associated physical properties (Demuzere et al., 2020a).

**Table 1.** A selection of urban canopy parameter data associated with built LCZ types, sourced from Stewart and Oke (2012). Columns represent the urban canopy parameters included in the thematic benchmark: the percentage of built ( $\lambda_B$  [%], ratio of building plan area to total plan area), impervious ( $\lambda_I$  [%], ratio of impervious plan area (paved, rock) to total plan area), and total impervious surface area ( $\lambda_T$  [%], defined as the ratio of the sum of the building and impervious plan areas to the total plan area), the mean height of roughness elements  $H$  [m] (geometric average of building heights), and the anthropogenic heat flux  $AHF$  [ $\text{W m}^{-2}$ ]. Maximum values for  $H$  (LCZs 1 and 4\*) and  $AHF$  (LCZ 10\*\*) are not available and are arbitrarily set to 200 m and  $1000 \text{ W m}^{-2}$  respectively.

LCZ	$\lambda_B$	$\lambda_I$	$\lambda_T$	<b>H</b>	<b>AHF</b>
1. Compact high-rise	40–60	40–60	>80	>25*	50–300
2. Compact midrise	40–70	30–50	>70	10–25	<75
3. Compact low-rise	40–70	20–50	>60	3–10	<75
4. Open high-rise	20–40	30–40	50–80	>25*	<50
5. Open midrise	20–40	30–50	50–90	10–25	<25
6. Open low-rise	20–40	20–50	40–90	3–10	<25
7. Lightweight low-rise	60–90	<20	>60	2–4	<35
8. Large low-rise	30–50	40–50	>70	3–10	<50
9. Sparsely built	10–20	<20	10–40	3–10	<10
10. Heavy industry	20–30	20–40	40–70	5–15	>300**

This approach is in line with previous regional works, that used datasets available for specific regions only, such as for Europe (Demuzere et al., 2019a) or the continental United States (Demuzere et al., 2020a). For the current study, (semi-)independent, consistent and open-source datasets with global coverage are selected, that are critical to distinguish the LCZ classes (surface

cover, packing and height of roughness elements, and thermal properties), and that are ideally representative for the year 2018. The various products are described first, followed by an explanation on how the thematic benchmark is performed.

- 225
- **Surface cover** is sourced from the Copernicus Global Land Cover Layers - Collection 3 (CGLCL3), a global discrete land cover map at 100 m resolution, available on a yearly basis from 2015 to 2019, of which 2018 is selected (Buchhorn et al., 2020a, b). These maps describe the Earth's terrestrial surface in up to 23 distinct land cover classes following the United Nations Land Cover Classification System (Di Gregorio, 2005). In contrast to the natural classes, which are primarily obtained via PROBA-V sensor data, the single urban class is largely identified using the World Settlement
- 230
- Footprint (WSF, Marconcini et al. (2020)) from DLR (German Aerospace Center), a global map of human settlements on Earth for the year 2015.
- **Packing of the roughness elements** can be characterised by the building ( $\lambda_B$ ), impervious ( $\lambda_I$ ), or total impervious ( $\lambda_T = \lambda_B + \lambda_I$ ) surface. Recent literature reports on a variety of products that claim to represent global impervious surfaces (e.g. Gong et al., 2020; Marconcini et al., 2020; Zhang et al., 2020a). These datasets generally adopt an urban
- 235
- mask approach; here we follow the European Environmental Agency's (EEA) definition of imperviousness density as 'the percentage of sealed artificial surface' (European Environment Agency, 2018a). In contrast, the global and high-resolution Sentinel-2 based probability of built-up areas (GHS-S2Net) provides a valuable alternative Corbane et al. (2021). GHS-S2Net is produced using a Convolution Neural Networks architecture for pixel-wise image classification that automatically extracts built-up areas at a spatial resolution of 10 m from a global composite of Sentinel-2 imagery
- 240
- (Corbane et al., 2020), representative for 2018. The dataset reports about built-up areas in the form of probabilities, indicating the probability of a pixel (values between 0-100) to belong to the built-up class. Moreover, based on an evaluation using building footprints from 277 regions across the globe, Corbane et al. (2021) indicated that there is a strong relationship between the output probabilities and the building densities, suggesting that the model outputs can be used as a proxy for  $\lambda_B$ . As an additional test, we regress the GHS-S2net built-up probabilities against EEA's
- 245
- 100 m imperviousness density (IMD, reflecting  $\lambda_T$ ) and share of built-up (SBU, reflecting  $\lambda_B$ ) layers for the year 2018 (European Environment Agency, 2018a, b), for the thirty largest European functional urban areas (FUAs, Schiavina et al. (2019), see also Appendix C). The results (described in Appendix D) indicate that the GHS-S2net built-up probabilities on average explain >90% of the observed  $\lambda_T$  and  $\lambda_B$  variability, with regression slopes closer to 1 for  $\lambda_B$ . Therefore, GHS-S2net built-up probabilities are used in this study as a proxy for  $\lambda_B$ .
- **Height of the roughness elements** (building height,  $H$ ) data is taken from the 3D building structure data (unpublished data, based on Li et al. (2020a)), a global 1 km<sup>2</sup> resolution database of building height, building footprint, and building volume estimated for the nominal year of 2015. The data is estimated using a random forest algorithm, based on a wide range input layers, including optical imagery (different Landsat bands), synthetic-aperture radar data from Sentinel-1, derivatives of remote sensing products (such as the enhanced vegetation and normalized difference vegetation indices),
- 250
- and other socio-economic data (road networks, DEM, Gross Domestic Product and Gini indices reflecting economic
- 255
- inequalities within cities, etc). In this product, building height denotes the average height of all buildings in a pixel,



weighted by the area of each building. As such, it does not consider ground surfaces (roads, parking places, etc.) and excludes other tall features such as trees. Building height is estimated only for areas (pixels) that include built-up land in the year 2015, according to the WSF data (Marconcini et al., 2020).

- 260 • **Anthropogenic heat** ( $AHF$ ) is the final LCZ attribute that can be evaluated; unfortunately there are no global databases of thermal and radiative properties of the urban fabric that can be used. Here, the recent 1 km<sup>2</sup> global  $AHF$  dataset from Varquez et al. (2021) is selected (hereafter referred to as AH4GUC) to benchmark the global LCZ map. AH4GUC is a freely available database (Varquez et al., 2020), contains maps of hourly and annual mean anthropogenic heat emissions representing the periods 2010s and 2050s (2010's annual mean is used here), and integrates anthropogenic  
265 heat emissions from primary energy consumption (e.g. industrial, agricultural, commercial, residential and transport sectors) and metabolic processes.

The thematic benchmark is performed for 150 selected urban regions (Fig. C1), which are identified by selecting the 10 most populated FUAs per urban ecoregion that are covered by the global LCZ map. In order to compare the surface cover (built versus natural) from CGLCL3 with the LCZ map, the latter is converted into a binary product; all built LCZs (except  
270 LCZ 9 - Sparsely built, which is predominantly natural) are converted to a single 'urban' class, and all remaining classes are considered as natural. A per-pixel quality assessment is then performed for each FUA, and is described in terms of the balanced accuracy (BA) - providing information about the rate of correctly classified pixels in an unbalanced setting where natural pixels are predominant compared to urban pixels - and Cohen's Kappa (CK) - that compensates for random chance in the pixels assignment (Corbane et al., 2021).

275

As can be seen from Table 1, the benchmark UCPs  $\lambda_B$ ,  $H$ , and  $AHF$  are characterised by value ranges (e.g.  $\lambda_B$  for LCZ 1 ranges between 40 and 60%), so that a one-to-one evaluation is not possible. As such, for each of the UCPs, the mapped LCZ classes are replaced by their corresponding minimum, mean and maximum UCP values, which are then regressed against the reference products described above. As observed  $H$  and  $AHF$  products are available on a 1 km<sup>2</sup> resolution, the 100 m LCZ-  
280 based minimum, mean and maximum UCP maps and 10 m GHS-S2Net urban probabilities are all resampled to a common 1 km<sup>2</sup> resolution. The resulting coefficients of determination ( $R^2$ ) and slopes are reported as measures for the LCZ-based UCP explanatory power.

### 3 Results

#### 3.1 Global LCZ map

285 Applying the TA curation procedure explained in Section 2.1 resulted in 410 ROIs, consisting out of 63.847 polygons and 2.018.916 pixels. Their distribution between ER varies (e.g. number of ROIs ranging between 8 and 100, for ER 11 - Tropical, sub-tropical grassland and ER 8 - Tropical, sub-tropical forest in Asia, respectively), in line with global population density patterns (Fig. 3). The number of TA polygons are well distributed across the different LCZ classes (Fig. E1), with lowest



numbers for LCZs 7 (Lightweight lowrise) and 1 (Compact highrise), and highest numbers for LCZs D (Low plants) and 6  
 290 (Open lowrise). It is interesting to note that, for most LCZ classes, the biggest share of TA polygons per LCZ class and urban  
 ecoregion comes from ROIs in ER 3 - Temperate forest in East Asia (Fig. E1), even though this ER only has an average number  
 of ROIs. This is in part caused by a small number of LCZ Generator submissions with a very high number of TAs, such as the  
 3000+ TAs for the larger Nanjing - Bengbu - Huai'an (People's Republic of China) submission (Pan, 2021).

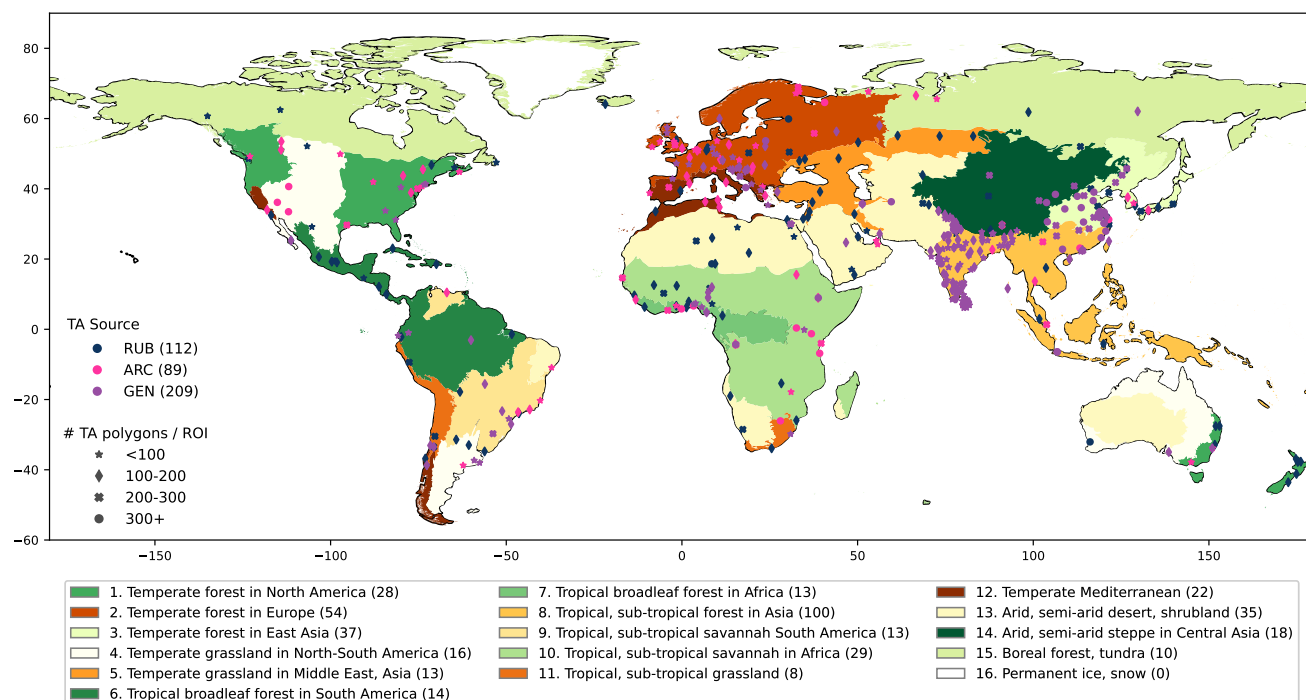


**Figure 3.** Spatial distribution of global TA sets on top of the urban ecoregions (ER), only showing the centroid of each ROI. Marker type reflects the amount of TA polygons per ROI, marker colors the TA source. Values between brackets in the TA source and ER legend indicate the number of ROIs per source and per ER, respectively. Note that ER colors and names are adopted from Schneider et al. (2010).

Alongside the curated TA samples, thirty earth observation input features are used in the classification procedure, an outcome  
 295 of the feature importance ranking procedure (Section 2.3). The sum average (savg) GLCM texture feature derived from PAL-  
 SAR's HV polarisation backscattering coefficients is found to be most important, followed by the newly developed NANTLI  
 metric and the 90th percentile of the Normalized Difference Vegetation Index (NDVI) multi-annual composite (Fig. F1). The  
 remainder of the selected features contain information about topography, Landsat 8 bands and band ratios, Sentinel-2 NDVI  
 band ratios, Sentinel-1 VV and VH composites, some other PALSAR HH and HV GLCM textures, and the Global Canopy  
 300 Forest Height (GCFH). For clarity, a final list of selected features and their description is provided in the Table F1. Finally, it  
 is worthwhile to note that the 16 discarded features only indicate a very limited contribution to the LCZ map quality across  
 all urban ecoregions. For example, six features never belong to the top 50% of the most important features (VVH, PAL-



SAR\_HH\_SHADE, ASPECT, S2\_sei\_median, S2\_csi\_median, and CHM), and another five only one time (S2\_B6\_median, S2\_B7\_median, S2\_rep\_median, VV\_HH and EBBI) (please refer to Table 2 in Demuzere et al. (2021b) for abbreviations).  
 305 This indicates the generic character of the selected earth observation input feature space that is able to cover the global (urban) land surface heterogeneity representative for different clusters of climate, vegetation, and urban topology.

The resulting 100 m spatial resolution global LCZ classification, based on all TAs and selected input features, is shown in Fig. 4. As LCZs were originally designed as a new framework for UHI studies Stewart and Oke (2012), they also contain a limited  
 310 set of ‘natural’ land-cover classes (LCZs A to G) that can be used as ‘control’ or ‘natural reference’ areas, which dominate the global view. However, the seven natural classes in the LCZ scheme can not capture the heterogeneity of the world’s existing natural ecosystems, and thus cannot match other products such as the 20, 36 or 75 layers that describe the Earth’s terrestrial surface in the Copernicus Global Land-Cover Layers (Buchhorn et al., 2020a, b), the European Space Agency Climate Change Initiative land-cover map (ESA, 2017), or the global map of terrestrial habitat types (Jung et al., 2020) respectively. In contrast,  
 315 the added value of the LCZ framework (and map) is the diversity of urban classes, which are easily interpretable and globally consistent, capturing the intra-urban variability of surface forms and land functions.

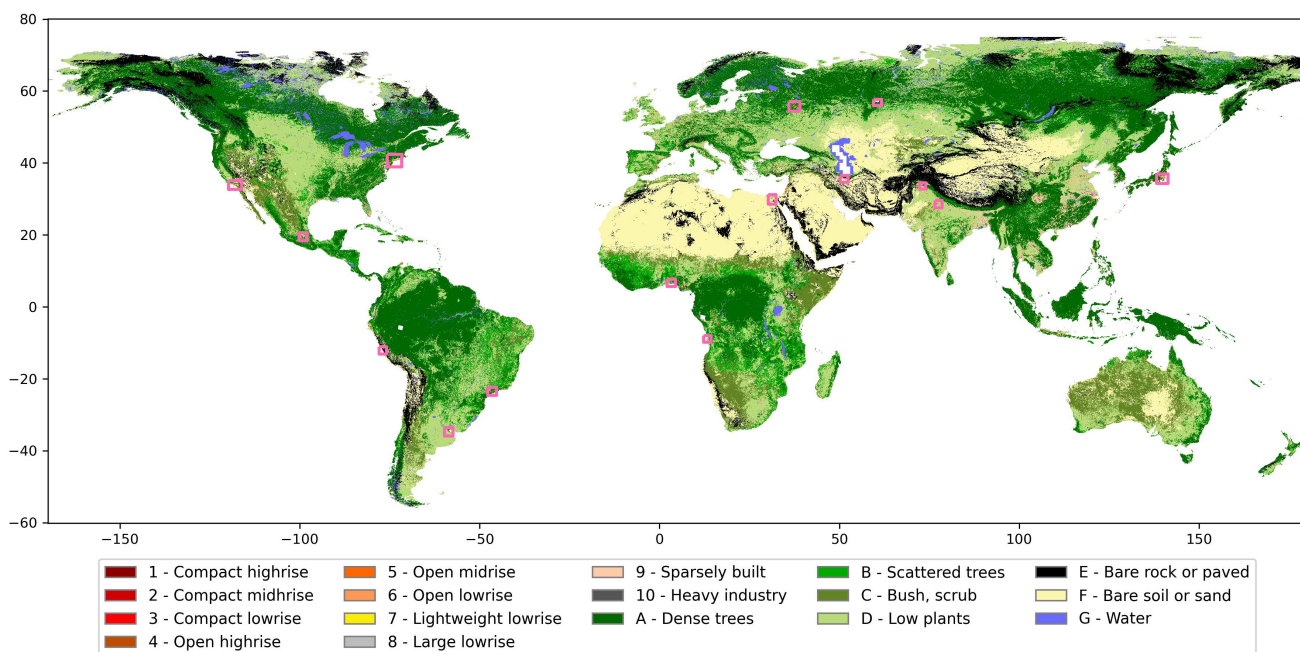


**Figure 4.** Global map of Local Climate Zones. Detailed views of the pink bounding boxes are shown in Figures 5, 6 and 7.

This is show-cased by zooming into the largest FUAs per urban ecoregion in Figures 5, 6 and 7, simultaneously showing the LCZ probabilities (discussed in Section 3.2) and corresponding binary CGLCL3 surface cover. The LCZ map for e.g. New York (ER1, Fig. 5) illustrates the compact high- and mid-rise areas clustered in and around Manhattan, more open and lower-



320 rise areas outwards of the city, and large-scale low-rise and industrial urban urban land cover around the Port of Newark west  
of Manhattan. A second example is the city of Moscow (ER2, Fig. 5) in which its concentric layout mainly hosts LCZs 1, 2  
and 4 in the centre, and LCZs 5 and 6 when moving to the suburbs and its satellite cities. Such information is crucial to e.g.  
characterise the UHI, as was recently demonstrated for Moscow by Varentsov et al. (2020, 2021), using the regional climate  
model COSMO-CLM, and observations from a dense network of around 80 reference stations augmented with more than 1.500  
325 crowd-sourced citizen weather stations. More in general, the global LCZ map allows to make such type of assessments for any  
global urban area, by moving away from the traditional urban mask and incorporating cities' internal make-up (Bechtel et al.,  
2017; Ching et al., 2018).

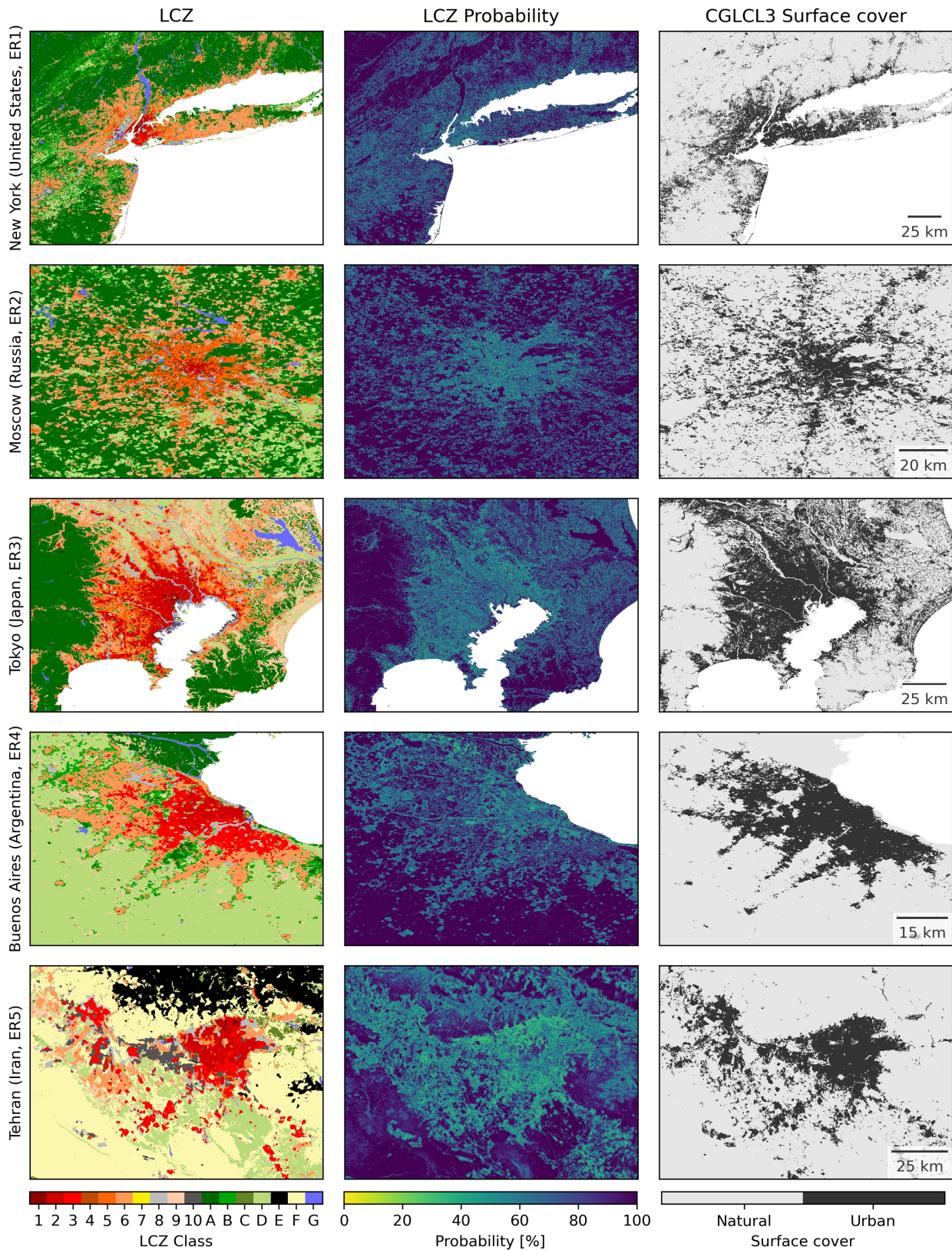


**Figure 5.** LCZ map, its probability and the corresponding binary CGLCL3 surface cover for the largest FUAs in urban ecoregions 1 to 5.

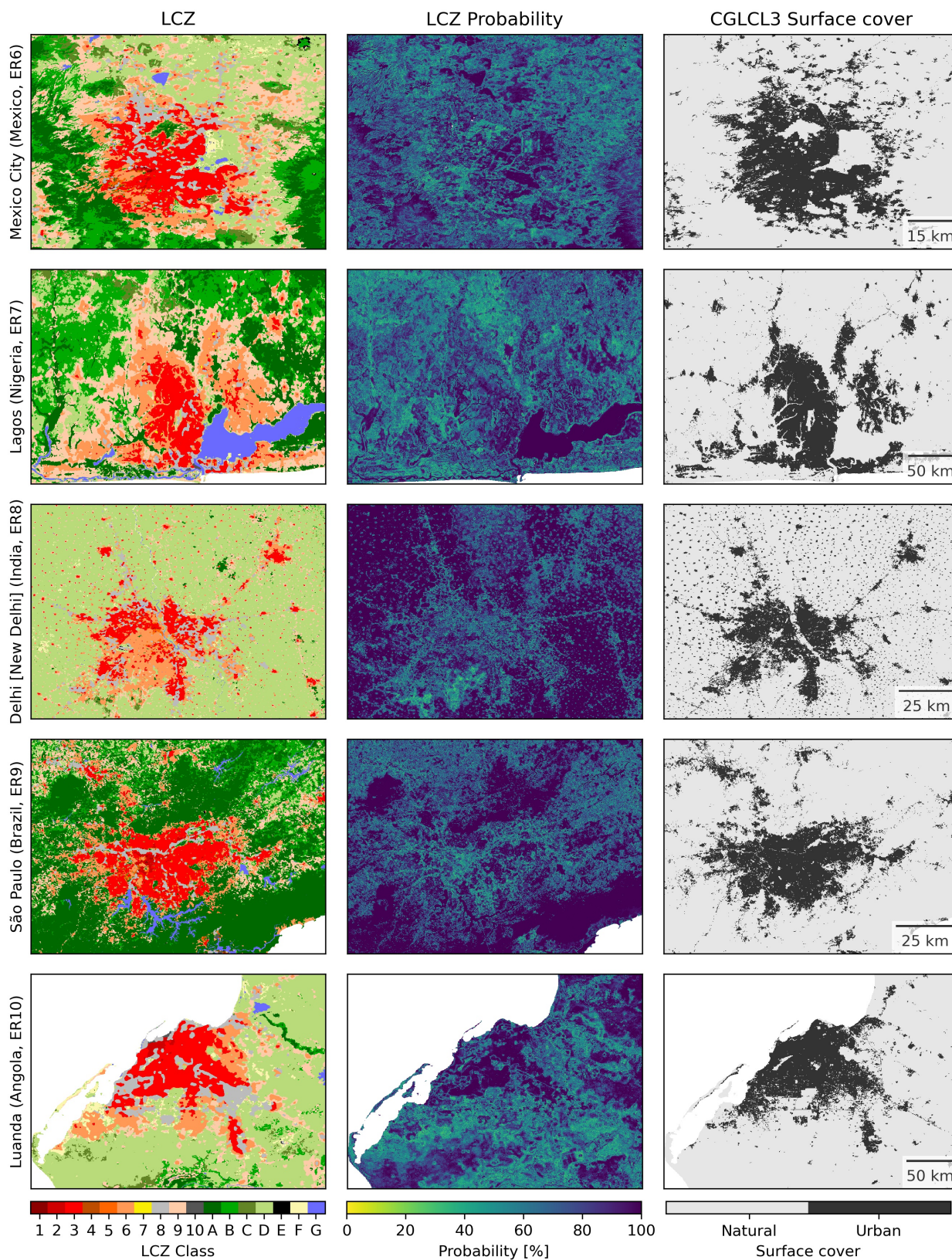


**Figure 6.** As Fig. 5 but for the largest FUAs in urban ecoregions 6 to 10.

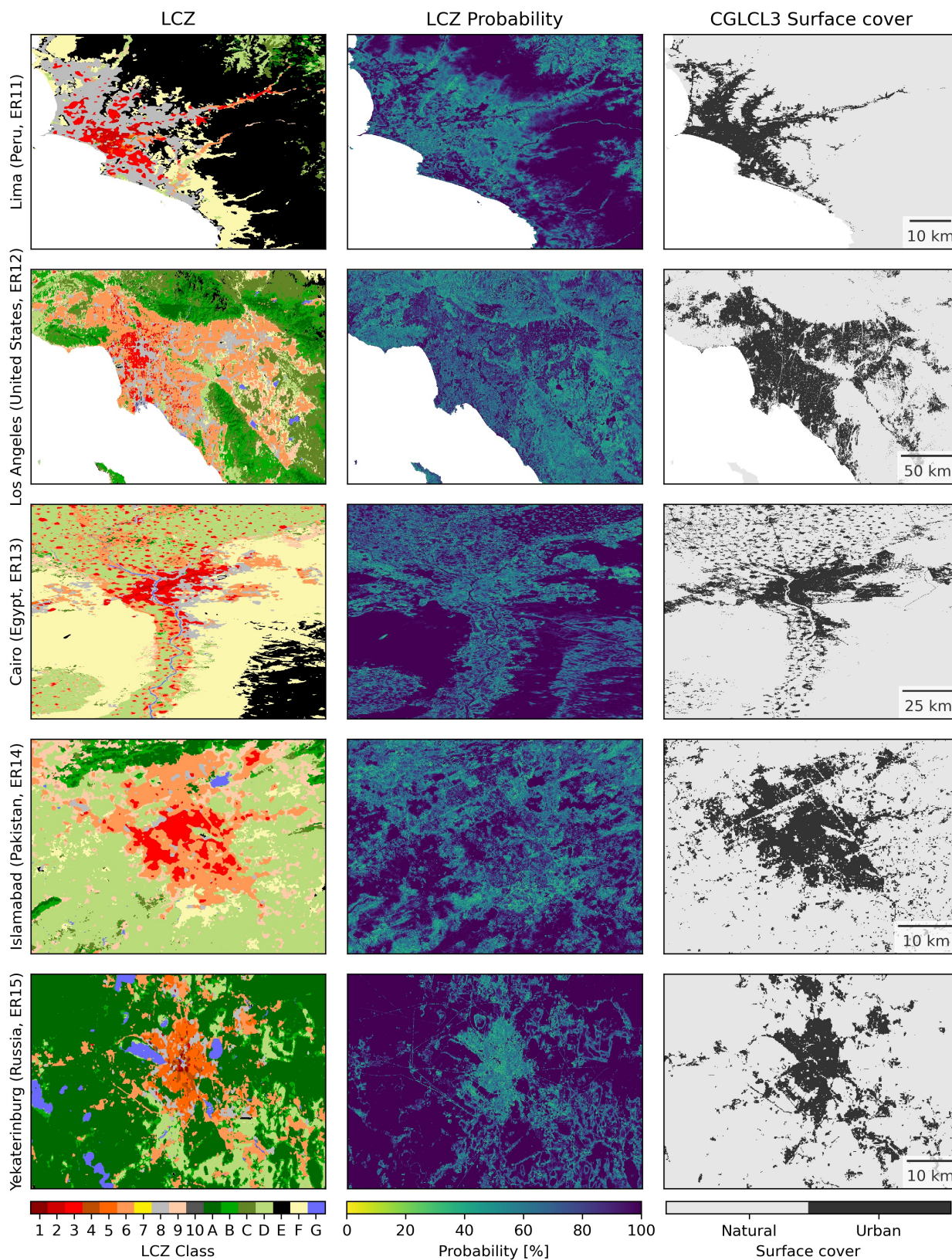


**Figure 7.** As Fig. 5 but for the largest FUAs in urban ecoregions 11 to 15.



Historic urbanisation patterns are the consequence of countless decisions made at building, neighbourhood and city scales. As such, cities have unique fingerprints reflecting distinct topographic, cultural and economic contexts. To assess the global differences of built forms and functions, the LCZ frequencies are first categorised in groups reflecting their degree of total impervious fraction. The HIGH- $\lambda_T$  cluster (LCZs 1, 2, 3 and 8) is characterised by average  $\lambda_T > 85\%$ , whilst the MEDIUM- $\lambda_T$  cluster (LCZs 4, 5, 6 and 9) typically has average  $\lambda_T$  values between 25% and 70%. A third cluster is added that groups LCZs 7 and 10, two LCZ classes that are distinct for their materials (LCZ 7) and anthropogenic heating (LCZ 10). The distribution of these clusters is then aggregated and visualised per urban ecoregion, enriched by their corresponding underlying LCZ classes and their lcz-based building height properties (Fig. 8). It is clear that there are fundamental geographic differences in the urban layout of cities: cities in e.g. ER 1 (Temperate forest in North America) are dominated by the open cluster, and more specifically LCZ 6. The small fraction taken by the compact cluster is in turn dominated by LCZ 8, reflecting large lowrise buildings - often commercial centers. In contrast, cities in ER 11 (Tropical, sub-tropical grassland) have a more balanced distribution of compact and open classes. Here, the compact class is mostly occupied by LCZs 3 and 8, and the open cluster by LCZs 6 and 9. One consistent pattern is however apparent: a clear domination of low-rise built forms across all urban ecoregions. The two most contrasting examples in this respect are ER 3, with a relevant share of LCZs 1, 2, 4 and 5, and ER 10 (Tropical, sub-tropical savannah in Africa) that is almost completely dominated by low-rise built forms.

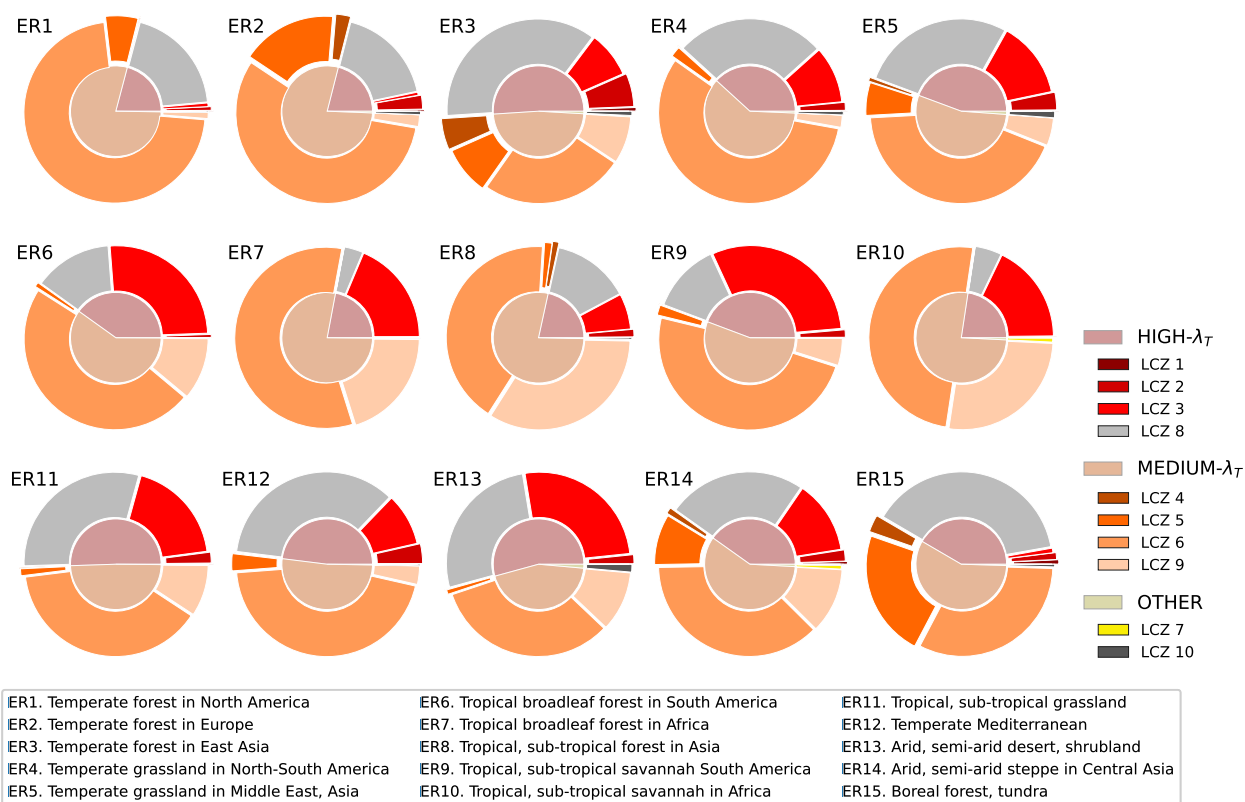


**Figure 8.** Distribution of the built LCZ classes for all 13.135 urban centres in the Urban Centre Database, aggregated per urban ecoregion. The inner rings indicate the HIGH (LCZs 1, 2, 3, and 8), MEDIUM (LCZs 4, 5, 6, and 9) and OTHER (LCZs 7 and 10) degree of total imperviousness ( $\lambda_T$ ) clusters. The outer rings depict the actual LCZ classes. The expansion of individual LCZ wedges visually reflects the differences in building height across LCZ classes (see Table 1).

### 3.2 Quality assessment and benchmarking

As part of the multiple lightweight global random forest models procedure described in Section 2.3, a global LCZ-probability layer is produced that identifies how often the modal LCZ was mapped (out of a total of 50 random forest results), indicating a first measure of robustness of the classification. This probability layer (in %) is shown in the middle panels of Fig. 5 for the largest FUA per urban ecoregion. Yet in order to get a more comprehensive overview, LCZ-based probabilities are aggregated over all 13.135 cities in the Global Human Settlement Layer Urban Centres Database (GHS-UCDB, Florczyk et al. (2019)). Mean probabilities across the globe are greater than 50% for all LCZ classes, meaning that the resulting modal LCZ class was mapped by more than half of the 50 LCZ models. Highest probability values are obtained for LCZs 6, 8, A (Dense trees) and G (Water) (~80 to 100 %), and lowest values are found for LCZs 1, 4, 5 and 7, which can be due to a variety of reasons. First, these LCZ types are typically characterised by a lower number of TAs, decreasing its potential weight in the random forest



models. Second, some of these LCZ classes are characterised by similar building footprints and impervious surface areas (e.g. LCZs 4 and 5), yet differ mainly in the height of their roughness elements (see Table 1). As a conscious decision was made to use the lower resolution building height dataset as a semi-independent benchmark dataset (described in Section 2.4.2), currently no input feature directly represents the roughness of buildings (See also Demuzere et al., 2019b, 2020a). In terms of the ER-stratified values, all probabilities per LCZ class are in line with the global values, demonstrating the universality of the LCZ typology and the robustness of the classifiers and input features across the urban ecoregions. Probabilities for LCZ 7 deviate from this behaviour (values < 40% for ER's 11 and 12), which might be due to relatively low number of ROIs and concurring lower number of TA polygons for LCZ 7. In addition, as this LCZ class includes informal settlements - often consisting of lightweight materials and densely packed buildings inter-spaced with hard-packed surfaces - these pixels present a challenge for the classifier because of their mixed spectral signature (Stewart, 2011b; Brousse et al., 2020a; Van de Walle et al., 2021, 2022). For this LCZ type, future versions of the global map might benefit and built further upon recent efforts dedicated to map informal urban settlements (see e.g. Kuffer et al., 2020; Assarkhaniki et al., 2021; Owusu et al., 2021; Abascal et al., 2022).

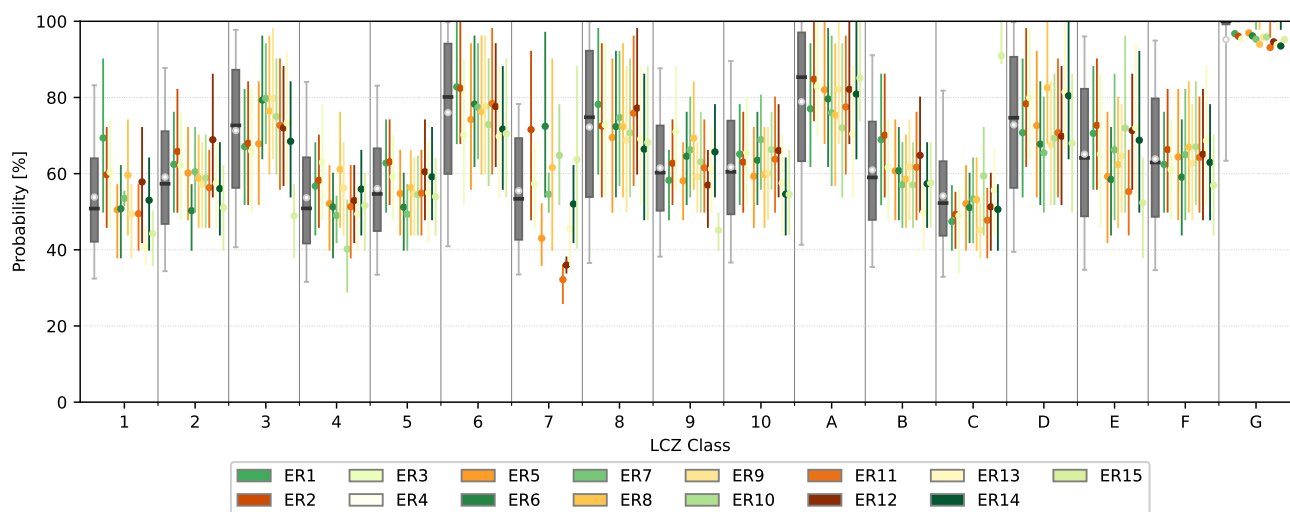


**Figure 9.** Probabilities of the mapped LCZ classes, aggregated over all GHS-UCDBs. The grey boxplots depict the probability distribution for all global urban centres, per LCZ class, with boxes and whiskers spanning the 25-75 and 5-95 percentiles respectively, and means and medians indicated by the white dots and black lines respectively. The ER-colored lines (color legend as in Fig. 3) indicate the 25 to 75th percentile range averaged over the urban centres, stratified per ER. ER-colored dots indicate the mean.

The traditional accuracy assessment using the independent training / test samples obtained via the ‘splitting the polygon pool’ approach (Xu et al., 2021) and the fifty lightweight random forest models results in scores of >70% for all OA metrics (Fig. G1). The variability across the fifty random forest models is small, indicating the robustness of the global classification protocol. Interestingly, the global OA values using the reduced set of final input features is higher compared to the accuracy



370 assessment using all input features ( $74.5\% \pm 15.1$ , Fig. F1), supporting the valid removal of uninformative input features from the multi-dimensional input feature space. The class-wise F1 metric shows larger variability with values for the built LCZs between 50% (LCZ 1 - Compact highrise) and 78% (LCZ 6 - Open lowrise), and  $>60\%$  for all natural classes. The lowest accuracy is obtained for LCZs 1, 4, 5, 7 and 10, in line with the results of the probability layer discussed above.

375 Since the LCZ typology is a representation of urban form - defined via the corresponding universal LCZ-based canopy parameters - a thematic benchmark allows to indirectly assess the quality of the LCZ map for continuous land surfaces, including those pixels not part of the TA samples used in the traditional accuracy assessment. Fig. 10(A) reveals a good correspondence between the built LCZ classes and the urban class from the CGLCL3 - taken from the World Settlement Footprint data (Marconcini et al., 2020) - with an average Balanced Accuracy (BA) and Cohen's Kappa (CK) of 90% and 73%, respectively.

380 Stratifying the BA results per urban ecoregion indicates a similar performance, with mean BA values ranging between 83% (ER3) and 93% (ER4) (Fig. H1). A similar variability can be observed for the CK results stratified per urban ecoregion, with mean CK values ranging between 65% (ER8) and 80% (ER9). These results indicate that the global LCZ map presents a good correspondence with a state-of-the-art and dedicated built-up land data product, and is thus able to correctly discriminate between built-up and natural land cover (confirmed independently by an  $OA_{bu}$  of  $\sim 95\%$ , an accuracy metric that evaluates the

385 built versus natural LCZ classes only (Fig. G1)).

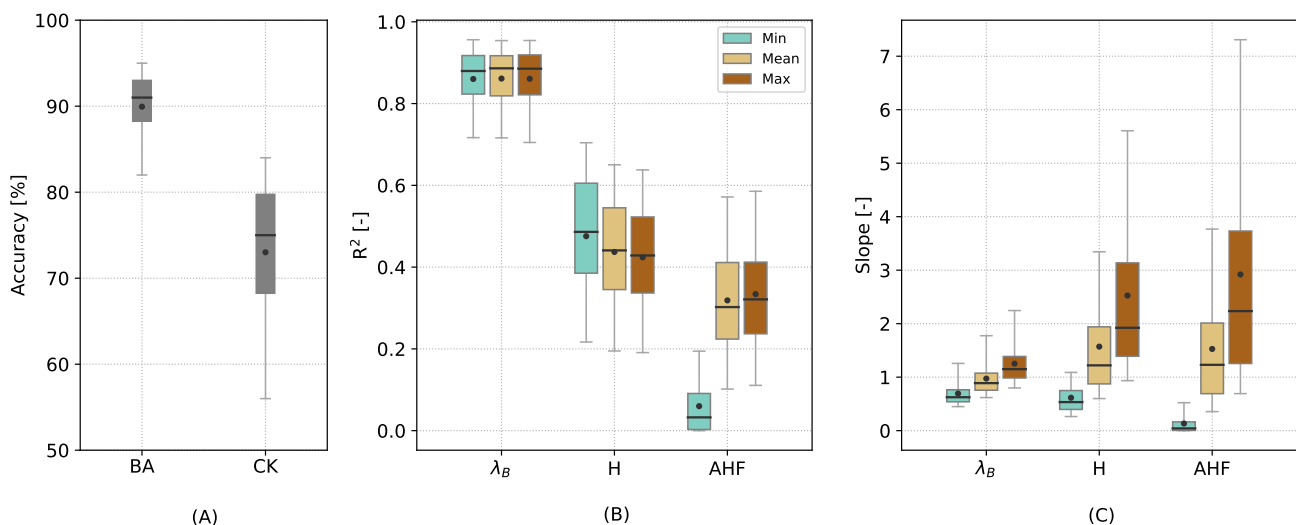


**Figure 10.** Results for the thematic benchmark, for (A) the CGLCL3 urban mask (A) and  $\lambda_B$ ,  $H$ , and  $AHF$  (B and C). All accuracies are derived for the 150 global LCZ FUA regions. For built-up land, accuracy is expressed using the Balanced accuracy (BA) and Cohen's Kappa (CK). For  $\lambda_B$ ,  $H$ , and  $AHF$ , the coefficients of determination ( $R^2$ ) (B) and slopes (C) result from the regression between the reference datasets and their corresponding universal LCZ-based values from Stewart and Oke (2012), using minimum, mean and maximum values (colours). For all panels, boxes and whiskers span the 25–75 and 5–95 percentiles respectively. The means and medians are indicated by the black dots and lines respectively. Results stratified per urban ecoregion are available in Appendix H.



For  $\lambda_B$ ,  $H$ , and  $AHF$  - characterized by UCP value ranges (Table 1) - a one-to-one evaluation with their reference datasets (described in Section 2.4.2) is not possible. As such, minimum, mean and maximum UCP values are regressed against these reference products, from which the coefficients of determination ( $R^2$ ) and slopes represent the measures of explanatory power of the LCZ map (Fig. 10B,C and Fig. H2 for results stratified per urban ecoregion). The LCZ-based building surface fraction  $\lambda_B$  is in very good agreement with the GHS-S2Net proxies, with mean  $R^2$  values close to 0.9 for the whole value range. Slope values provide a slightly more nuanced result, with average values 0.69, 1 and 1.22 when targeting the minimum, mean and maximum  $\lambda_B$  UCP values. In other words, assigning the means of the  $\lambda_B$  value ranges to each corresponding LCZ class is a very good approximation for the building surface fraction for global cities. Results for building heights  $H$  and the anthropogenic heat flux  $AHF$  can be interpreted in the same way (Fig. 10B,C and Figures H3 and H4 for results stratified per urban ecoregion). For  $H$ ,  $R^2$  / slope values range between 0.42 / 2.5 and 0.5 / 0.59 for the maximum and minimum LCZ-based  $H$  values. Also here, the best results are obtained using the mean of the LCZ-based value ranges, even though only  $\sim 50\%$  of the observed building height is explained, and the mean LCZ-based values tend to overestimate the reference values. For  $AHF$ , it is clear that assigning the minimum of the LCZ-based  $AHF$  range to the LCZ map has little explanatory power:  $R^2$  is 0.1 with a slope of  $\sim 0.1$ . Slightly better results are obtained when using the maximum and especially the mean of the  $AHF$  value range, but also here only 30% of the observed  $AHF$  variability can be explained by the LCZ map. From previous anthropogenic heat flux works (Oke et al., 2017) it is clear that this is not surprising. The  $AHF$  values provided by Stewart and Oke (2012) are fixed ranges, reflecting the mean annual heat flux density from fuel combustion and human activity (transportation, space cooling/heating, industrial processing, human metabolism) at the local scale. Yet as also indicated in their Table 4 (footnote c), these values vary significantly with latitude, season, and population density. LCZs have previously been shown to indirectly capture information on population densities (Demuzere et al., 2020a), and also the role of seasonality with respect to LCZ-based annual  $AHF$  values has been discussed elsewhere (e.g. Varentsov et al. (2020)). Yet it is obvious that the observed zonal  $AHF$  variability in AH4GUC (Varquez et al., 2021, their Fig. 5) is neglected completely in this thematic benchmark. This means that, for example, an LCZ 6 neighbourhood in tropical Singapore will be assigned the same mean annual  $AHF$  values as an LCZ 6 area in the high-latitude city of Helsinki (Finland), even though it is clear that their building cooling / heating patterns will be completely different (Quah and Roth, 2012; Karsisto et al., 2016). This reveals a strong limitation of using  $AHF$  as an independent benchmark of the global LCZ map. Unfortunately, as there are currently no globally explicit databases on thermal and radiative properties of the urban fabric,  $AHF$  is currently the only available proxy to indirectly assess the ‘thermal’ signature of a built environment. Finally, there are a number of other elements that might affect deviations between the LCZ-based UCP parameters and their benchmark products and comparison methods: some benchmark products are merely indirect observations (e.g. GHS-S2Net urban probabilities being used as a measure for  $\lambda_B$ ), UCPs might have dissimilar definitions (e.g. geometric average of buildings heights versus average of building heights weighted by building footprint), or data matching differences as a consequence of different resolutions and map projections leading to potential artefacts from resampling.



#### 4 Serving earth system modelling and urban scale environmental science

420 Despite the new focus on cities as a critical scale for climate change risk management, we know very little about most cities  
on the planet - being generally ignorant of their extent, how they are constructed and how they are occupied (Demuzere et al.,  
2020a). This knowledge gap is especially true for urban areas in the Global South, where 90% of the projected world population  
growth of 2.5 billion over the next couple of decades will occur. This is in strong contrast with current urban knowledge that is  
predominantly shaped by research on and from the Global North (Nagendra et al., 2018). The global Local Climate Zone map  
425 presented here provides a globally consistent and climate-relevant urban description, that is an important prerequisite for de-  
veloping fit-for-purpose integrated climate-sensitive urban planning policies (Georgescu et al., 2015). As LCZs are developed  
from generalised perspectives of built forms and land cover types that are universally recognised and applicable (Stewart and  
Oke, 2012), this global LCZ map provides standardised and harmonised data of all cities, allowing to consistently assess the  
heterogeneous nature of cities' urban forms and functions, and providing the much-needed platform for comparative analyses,  
430 systematic learning and horizontal knowledge exchange between cities and regions (Raven et al., 2018; Ching et al., 2018; Bai  
et al., 2018; Creutzig et al., 2019; Reba and Seto, 2020).

As cities are complex systems and their components are difficult to understand in isolation, fundamental scaling laws that  
seem universal across cities are often put forward to understand their dynamics, growth and evolution in a scientifically pre-  
435 dictable, quantitative way (Bettencourt et al., 2007, 2020). In this work, city growth, structures and functions (e.g. urban area,  
albedo, population density, building density, building heights, anthropogenic heat flux, and sky view factor) are completely  
represented by population and universal scaling laws (Schläpfer et al., 2015; Manoli et al., 2019; Martilli et al., 2020). Other  
work has explored the correspondence between population density and carbon dioxide emissions (Ribeiro et al., 2019) and the  
allometric-scaling relationships between settlement population and non-point-source emissions of air pollutants (MacKenzie  
440 et al., 2019). In reality, the global universality of these scaling laws is unknown as many are created based on regional infor-  
mation only, mostly for data rich parts of the world (Bettencourt and West, 2010). Currently, city population is often used as  
proxy for urban form but the global LCZ map offers a richer alternative. In addition, the combination of population and LCZ  
may provide deeper insights into the variations of form in different cultural, socioeconomic and climatic contexts, and help  
guide future urban development. Since LCZs distinguish urban areas based on their form, the global map provides the means  
445 to assess the universality of the above-mentioned scaling laws, and refine/improve them. In addition, the global LCZ map has  
value beyond climate applications when combined with other spatially resolved urban information (Reba and Seto, 2020), like  
flooding hazard, biodiversity and air quality, for example.

Since the LCZ typology was initially designed for urban temperature studies (Stewart and Oke, 2012), typical applications  
450 focus on the UHI, usually providing the context for designing and analysing observations from urban meteorological networks  
(Skarbit et al., 2017; Beck et al., 2018; Chieppa et al., 2018; Verdonck et al., 2018; Yang et al., 2018; Leconte et al., 2020;  
Milošević et al., 2021; Zhang et al., 2020b; Zong et al., 2021), from crowdsourced data (Fenner et al., 2017; Varentsov et al.,



2021; Fenner et al., 2021) or from remote sensing (Wang and Ouyang, 2017; Bechtel et al., 2019b; Eldesoky et al., 2021; Stewart et al., 2021). However, the typology has been used for other purposes (see also Lehnert et al. (2021) for European applications), such as urban heat (risk) assessment studies (Verdonck et al., 2019b; Van de Walle et al., 2022), climate sensitive design, land use/land cover change, and urban planning (policies) (Perera and Emmanuel, 2018; Aminipouri et al., 2019; Vandamme et al., 2019; Maharroof et al., 2020; Chen et al., 2021b; Cai et al.), anthropogenic heat, building energy demand and consumption, and carbon emissions (Wu et al., 2018; Santos et al., 2020; Yang et al., 2020; Benjamin et al., 2021; Kotharkar et al., 2022), quality of life (Sapena et al., 2021), urban ventilation (Zhao et al., 2020b), air quality (Steenefeld et al., 2018; Lu et al., 2021a), urban vegetation phenology and ecosystem patterns, functions and dynamics (Kabano et al., 2021; Zhao et al., 2022), and epidemiological studies (Brousse et al., 2019, 2020a).

The LCZ scheme is a core element of the WUDAPT project to provide consistent urban data to support climate science (Ching et al., 2018, 2019) and many modelling systems nowadays ingest the LCZ typology, such as e.g. the Surface Urban Energy and Water Balance Scheme (SUEWS, Alexander et al. (2015, 2016)), UrbClim (Verdonck et al., 2018, 2019b; Sharma et al., 2019; Gilabert et al., 2020), the Vertical City Weather Generator (Moradi et al., 2022), ENVI-met (Middel et al., 2014; Lyu et al., 2019; Bande et al., 2020), the urban multi-scale environmental predictor (UMEP, Lindberg et al. (2018)), MUK-LIMO\_3 (Bokwa et al., 2019; Matsaba et al., 2020; Gál et al., 2021), COSMO-CLM and the WUDAPT-TO-COSMO tool (Wouters et al., 2016; Brousse et al., 2019, 2020b; Varentsov et al., 2020; Van de Walle et al., 2021), and the Weather Research and Forecasting model (WRF, Brousse et al. (2016); Hammerberg et al. (2018); Molnár et al. (2019); Pellegatti Franco et al. (2019); Wong et al. (2019); Mu et al. (2020); Zonato et al. (2020); Patel et al. (2020); Demuzere et al. (2021a); Hirsch et al. (2021); Patel et al. (2022)). Most studies focus on individual cities, with the work of Patel et al. (2022) being an exception as it uses the European LCZ map ((Demuzere et al., 2019a)) to simulate a continental-scale heat wave event. The LCZ map presented here allows the extraction of urban data suited to the scale of study and can support global climate and earth system modellings.

Regional climate models are expected to remain indispensable tools that complement global models for understanding physical processes governing regional climate variability and change (Gutowski et al., 2020). Yet at the same time, regional climate model developments also serve as a precursor for the evolution of global climate models, and major efforts are currently underway to increase ESMs to kilometre-scale resolutions (Schär et al., 2020; Bauer et al., 2021). Recently, Fuhrer et al. (2018) performed a near-global climate simulation at a horizontal grid spacing of just 930 m. Such advancements will represent a quantum jump in (urban) global climate modelling, enabling the explicit treatment of the complex interactions between the fine-grained urban heterogeneity and its atmosphere (Martilli et al., 2020). To date however, climate projections focused on built landscapes are absent, partly owing to the lack of climate-relevant urban data for ESMs (Zhao et al., 2021; Hertwig et al., 2021). Only one ESM included details of urban form in CMIP5<sup>3</sup> (Zhao et al., 2021), and a few more in CMIP6: except for GFDL-ESM (Dunne et al., 2020), these CMIP6 ESMs all use the Community Land Model-Urban (CLMU) urban canopy parameterisation (Oleson and Feddema, 2020). Yet despite its pole position, CLMU's lead developers indicate that transitioning

<sup>3</sup>Coupled Model Intercomparison Project, led by the World Climate Research Programme (<https://www.wcrp-climate.org/wgcm-cmip>)



to the LCZ urban classes and their corresponding UCPs will likely be beneficial for better simulating the interactions between the urban fabric and the climate system (Oleson and Feddema, 2020). Eventually, a more close connection between the global LCZ map and the ESM community might have a direct impact on climate change policies, via IPCC's<sup>4</sup> upcoming 7th cycle of  
490 Assessment Reports and its planned Special Reports on Cities and Climate Change.

Even though the LCZ typology presents a leap forward in describing intra-urban heterogeneity in a universal manner, its generalisation of course also has its limitations. In the words of Stewart and Oke (2012): "it's view of the landscape universe is highly reductionist [...] and LCZs represent a simple composition of buildings, roads, plants, soils, rock, and water, each in  
495 varying amounts and each arranged uniformly into 17 recognisable patterns. The 17 patterns should nevertheless be familiar to users in most cities, and should be adaptable to the local character of most sites". This multi-urban class typology follows the discourse of most categorical mapping efforts discussed elsewhere (Coops and Wulder, 2019), such that individual LCZ classes are each physically discrete in surface structure and land cover, leading to well-defined boundaries separating most classes. However, users of LCZs must always accept that the internal homogeneity portrayed by each class is unlikely to be found  
500 in the real world, but that the attempt to classify surface complexity in cities represents a key advancement in urban climate science (Stewart and Oke, 2012). It also represents a helpful starting point for more detailed studies of urban form and function at smaller spatial scales. Likewise, due to its reductionist character, the landscape universe represented by the 17 LCZ classes is not complete for several reasons. First we do not apply the subclass scheme, which allows mixture of several LCZ types but reduces its universality. Secondly, some landscapes such as extensive greenhouses are not included in the scheme, since they  
505 are unlikely to be selected for urban heat island studies. Moreover, the scale of real urban structures does not always match the climatic definition of local scale. However, we are convinced that the scheme is the best compromise between climatic variation and generic description of urban structures.

This first version of the global LCZ map itself also has limitations. For example, LCZ 7 requires more attention and alter-  
510 native mapping strategies, as discussed in Section 3.2. Confusion may also exist between classes with similar surface fractions (e.g. LCZs 3 and 8), especially if built materials have similar spectral properties (see e.g. LCZ map for Lima (Peru, ER11), Fig 7). Similarly, also the confusion between classes with similar surface fractions yet different height of roughness elements might be improved in the future. Note that the LCZ map also inherits shortcomings of the many global earth observation input features upon which it is built, such as for example, some missing data in areas that are frequently covered in clouds, or gaps  
515 in coverage because of changing satellite duty cycles. Such limitations can be addressed in future releases of the map, e.g. by harvesting the growing number of TA samples submitted to the LCZ Generator (which received more than 1.500 submissions in less than one year of operation), ingesting more and new high-resolution (earth observation) datasets when available, or by implementing alternative scalable classification algorithms (e.g. Yokoya et al., 2018; Yoo et al., 2020; Rosentreter et al., 2020). Nevertheless, from many above-mentioned examples and applications it is clear that this global LCZ map has a lot of  
520 potential serving urban and climate sciences at various scales. The map is universal and allows for comparisons between global

---

<sup>4</sup>The Intergovernmental Panel on Climate Change



regions. Yet at the same time it is flexible enough to allow anyone to adapt it to suit their purpose, using for example user- and site-specific LCZ-based UCP value if available (Ching et al., 2018). In other words, the global LCZ map describes all the cities of the world in the same, universal language, but interested users can read it in their own dialect. Finally, this development will also support future large-scale dynamic LCZ mapping efforts. Such examples to date are rare and focus on targeted cities  
525 (e.g. Vandamme et al., 2019; Wang et al., 2019; Demuzere et al., 2020b; Zhao et al., 2020a; Lu et al., 2021b; Cai et al.), yet they reveal a large potential in terms of characterising the temporal transformations of urban morphologies across and within different cities, identify the main drivers of such changes, and bridge the gap between policy making and urbanisation patterns, required to come up with informed, data-driven and rational urban planning strategies toward sustainable city developments.

## 5 Conclusions

530 Since their introduction in 2012, Local Climate Zones (LCZs) have become a standard for characterising urban landscapes according to climate-relevant properties of the surface. From that point forward, the number of applications using this universal urban typology has been growing exponentially, revealing the relevance and potential for a wide range of urban sciences. One of the typology's most popular uses is digital mapping, which can generate UCPs at the city scale for input to numerical climate models. However, the lack of available and consistent global data on the form and function of cities has impeded progress in  
535 urban climate sciences so far, limiting applications to cities or regions for which LCZ maps are currently available.

The 100 m resolution global LCZ map presented here is the first of its kind depicting the much needed global intra-urban heterogeneity in an universal language. It allows easy access to Local Climate Zone data for regional and global scale analysis and provides a seamless integration into existing topographic, natural land cover, and other global scale data products. The map  
540 is generated building further upon previous studies, whilst adding new methodological features that balance optimal learning across global climates and urban typologies with accuracy, computational feasibility and efficiency.

Since this global map identifies the relevant data for planning and climate on neighbourhood, city and global scales, its designed to become part of a basic infrastructure to support a host of studies on exposure to environmental hazards, energy  
545 demand, climate adaptation and mitigation solutions and human health, as examples.

## 6 Data availability

The global Local Climate Zone map, representative for the nominal year 2018 and with a spatial resolution of  $\sim 100$  m (EPSG:4326), is available from <http://doi.org/10.5281/zenodo.6364594> (Demuzere et al., 2022a). The dataset contains various layers stored as separate GeoTIFF files, including: (1) `lcz_filter`, the recommended global LCZ map after applying the  
550 morphological Gaussian filter described in Demuzere et al. (2020a), (2) `lcz`, as (1), but presenting the raw LCZ map before applying the morphological Gaussian filter, and (3) the LCZ probability layer (%) that identifies how often the modal



LCZ from (2) was chosen per pixel. The LCZ maps have the default WUDAPT LCZ color scheme embedded (Fig. 1), and all imagery can be processed using (free) GIS software, e.g. QGIS. In addition, a teaser sample is provided to ease accessibility, providing the LCZ map information for the 15 largest functional urban areas stratified by urban ecoregion. These  
555 GeoTIFF files reflect the underlying data used in Figures 5, 6 and 7 of the manuscript. This teaser dataset is available from <https://doi.org/10.5281/zenodo.6364705> (Demuzere et al., 2022b).

*Author contributions.* MD designed the research, with feedback from BB and JK. The RUB training area samples were mostly digitised by CM. JK provided technical support with respect to the LCZ Generator database. MD performed all analysis and developed all visualisations. MD wrote the original draft, with contributions from all other authors.

560 *Competing interests.* The authors declare no competing interest.

*Acknowledgements.* We acknowledge all WUDAPT contributors and community members for providing the training areas via the portal or the LCZ Generator, with a special thanks to Samira Safae and Dev Niyogi for providing the large sample of Indian cities. We thank USGS and NASA for the free Landsat data, and the Copernicus programme of ESA for the Sentinel data, all acquired and processed via Google's earth engine. We also like to thank all research institutes and universities for the creation and provision of open datasets, such as  
565 the Copernicus Global Land Cover Layers, the Sentinel-2 based probability of built-up areas, and the anthropogenic heat flux data. Finally, we acknowledge support by the Open Access Publication Funds of the Ruhr-Universität Bochum (RUB, Germany).

*Financial support.* This work was conducted in the context of project ENLIGHT, funded by the German Research Foundation (DFG) under grant No. 437467569. JvV is supported by the Netherlands Organisation for Scientific Research, grant no. VI.vivi.198.008, Guiding human settlements towards sustainable urbanisation.



## 570 References

- Abascal, A., Rothwell, N., Shonowo, A., Thomson, D. R., Elias, P., Elsey, H., Yeboah, G., and Kuffer, M.: “Domains of deprivation framework” for mapping slums, informal settlements, and other deprived areas in LMICs to improve urban planning and policy: A scoping review, *Computers, Environment and Urban Systems*, 93, 101–170, <https://doi.org/10.1016/j.compenvurbsys.2022.101770>, 2022.
- Alexander, P., Bechtel, B., Chow, W., Fealy, R., and Mills, G.: Linking urban climate classification with an urban energy and water budget  
575 model: Multi-site and multi-seasonal evaluation, *Urban Climate*, 17, 196–215, <https://doi.org/10.1016/j.uclim.2016.08.003>, 2016.
- Alexander, P. J., Mills, G., and Fealy, R.: Using LCZ data to run an urban energy balance model, *Urban Climate*, 13, 14–37, <https://doi.org/10.1016/j.uclim.2015.05.001>, 2015.
- Aminipouri, M., Knudby, A. J., Krayenhoff, E. S., Zickfeld, K., and Middel, A.: Modelling the impact of increased street tree  
580 cover on mean radiant temperature across Vancouver’s local climate zones, *Urban Forestry and Urban Greening*, 39, 9–17, <https://doi.org/10.1016/j.ufug.2019.01.016>, 2019.
- Assarkhaniki, Z., Sabri, S., and Rajabifard, A.: Using open data to detect the structure and pattern of informal settlements: an outset to support inclusive SDGs’ achievement, *Big Earth Data*, 5, 497–526, <https://doi.org/10.1080/20964471.2021.1948178>, 2021.
- Bai, X., Dawson, R. J., Ürge-Vorsatz, D., Delgado, G. C., Barau, A. S., Dhakal, S., Dodman, D., Leonardsen, L., Masson-Delmotte, V.,  
Roberts, D., and Schultz, S.: Six research priorities for cities, *Nature*, 555, 23–25, <https://doi.org/10.1038/d41586-018-02409-z>, 2018.
- 585 Baklanov, A., Grimmond, C., Carlson, D., Terblanche, D., Tang, X., Bouchet, V., Lee, B., Langendijk, G., Kolli, R., and Hovsepyan, A.: From urban meteorology, climate and environment research to integrated city services, *Urban Climate*, 23, 330–341, <https://doi.org/10.1016/j.uclim.2017.05.004>, 2018.
- Bande, L., Manandhar, P., Ghazal, R., and Marpu, P.: Characterization of Local Climate Zones Using ENVI-met and Site Data in the City of Al-Ain, UAE, *International Journal of Sustainable Development and Planning*, 15, 751–760, <https://doi.org/10.18280/ijstdp.150517>, 2020.
- 590 Barlow, J. F.: Progress in observing and modelling the urban boundary layer, *Urban Climate*, 10, 216–240, <https://doi.org/10.1016/j.uclim.2014.03.011>, 2014.
- Bauer, P., Stevens, B., and Hazeleger, W.: A digital twin of Earth for the green transition, *Nature Climate Change*, 11, <https://doi.org/10.1038/s41558-021-00986-y>, 2021.
- Bechtel, B. and Daneke, C.: Classification of local climate zones based on multiple earth observation data, *IEEE Journal of Selected Topics  
595 in Applied Earth Observations and Remote Sensing*, 5, 1191–1202, <https://doi.org/10.1109/JSTARS.2012.2189873>, 2012.
- Bechtel, B., Alexander, P., Böhner, J., Ching, J., Conrad, O., Feddema, J., Mills, G., See, L., and Stewart, I.: Mapping Local Climate Zones for a Worldwide Database of the Form and Function of Cities, *ISPRS International Journal of Geo-Information*, 4, 199–219, <https://doi.org/10.3390/ijgi4010199>, 2015.
- Bechtel, B., Demuzere, M., Sismanidis, P., Fenner, D., Brousse, O., Beck, C., Van Coillie, F., Conrad, O., Keramitsoglou, I., Middel, A., Mills,  
600 G., Niyogi, D., Otto, M., See, L., and Verdonck, M.-L.: Quality of Crowdsourced Data on Urban Morphology—The Human Influence Experiment (HUMINEX), *Urban Science*, 1, 15, <https://doi.org/10.3390/urbansci1020015>, 2017.
- Bechtel, B., Alexander, P. J., Beck, C., Böhner, J., Brousse, O., Ching, J., Demuzere, M., Fonte, C., Gál, T., Hidalgo, J., Hoffmann, P., Middel, A., Mills, G., Ren, C., See, L., Sismanidis, P., Verdonck, M.-L., Xu, G., and Xu, Y.: Generating WUDAPT Level 0 data – Current status of production and evaluation, *Urban Climate*, 27, 24–45, <https://doi.org/10.1016/j.uclim.2018.10.001>, 2019a.
- 605 Bechtel, B., Demuzere, M., Mills, G., Zhan, W., Sismanidis, P., Small, C., and Voogt, J.: SUHI analysis using Local Climate Zones—A comparison of 50 cities, *Urban Climate*, 28, 100–145, <https://doi.org/10.1016/j.uclim.2019.01.005>, 2019b.



- Bechtel, B., Demuzere, M., and Stewart, I. D.: A Weighted Accuracy Measure for Land Cover Mapping: Comment on Johnson et al. Local Climate Zone (LCZ) Map Accuracy Assessments Should Account for Land Cover Physical Characteristics that Affect the Local Thermal Environment. *Remote Sens.* 2019, 11, 2420, *Remote Sensing*, 12, 1769, <https://doi.org/10.3390/rs12111769>, 2020.
- 610 Beck, C., Straub, A., Breitner, S., Cyrus, J., Philipp, A., Rathmann, J., Schneider, A., Wolf, K., and Jacobeit, J.: Air temperature characteristics of local climate zones in the Augsburg urban area (Bavaria, southern Germany) under varying synoptic conditions, *Urban Climate*, 25, 152–166, <https://doi.org/10.1016/j.uclim.2018.04.007>, 2018.
- Benjamin, K., Luo, Z., and Wang, X.: Crowdsourcing Urban Air Temperature Data for Estimating Urban Heat Island and Building Heating/Cooling Load in London, *Energies*, 14, 5208, <https://doi.org/10.3390/en14165208>, 2021.
- 615 Bettencourt, L. and West, G.: A unified theory of urban living, *Nature*, 467, 912–913, <https://doi.org/10.1038/467912a>, 2010.
- Bettencourt, L. M., Lobo, J., Helbing, D., Kühnert, C., and West, G. B.: Growth, innovation, scaling, and the pace of life in cities, *Proceedings of the National Academy of Sciences of the United States of America*, 104, 7301–7306, <https://doi.org/10.1073/pnas.0610172104>, 2007.
- Bettencourt, L. M., Yang, V. C., Lobo, J., Kempes, C. P., Rybski, D., and Hamilton, M. J.: The interpretation of urban scaling analysis in time, *Journal of the Royal Society Interface*, 17, <https://doi.org/10.1098/rsif.2019.0846>, 2020.
- 620 Biljecki, F., Chew, L. Z. X., Milojevic-Dupont, N., and Creutzig, F.: Open government geospatial data on buildings for planning sustainable and resilient cities, <http://arxiv.org/abs/2107.04023>, 2021.
- Bokwa, A., Geletič, J., Lehnert, M., Žuvela-Aloise, M., Hollósi, B., Gál, T., Skarbit, N., Dobrovolný, P., Hajto, M. J., Kielar, R., Walawender, J. P., Šťastný, P., Holec, J., Ostapowicz, K., Burianová, J., and Garaj, M.: Heat load assessment in Central European cities using an urban climate model and observational monitoring data, *Energy and Buildings*, 201, 53–69, <https://doi.org/10.1016/j.enbuild.2019.07.023>, 2019.
- 625 Breiman, L.: Random Forests, *Machine Learning*, 45, 5–32, 2001.
- Brousse, O., Martilli, A., Foley, M., Mills, G., and Bechtel, B.: WUDAPT, an efficient land use producing data tool for mesoscale models? Integration of urban LCZ in WRF over Madrid, *Urban Climate*, 17, 116–134, <https://doi.org/10.1016/j.uclim.2016.04.001>, 2016.
- Brousse, O., Georganos, S., Demuzere, M., Vanhuyse, S., Wouters, H., Wolff, E., Linard, C., and Lipzig, N. P. V.: Urban Climate Using Local Climate Zones in Sub-Saharan Africa to tackle urban health issues, *Urban Climate*, 27, 227–242, <https://doi.org/10.1016/j.uclim.2018.12.004>, 2019.
- 630 Brousse, O., Georganos, S., Demuzere, M., Dujardin, S., Lennert, M., Linard, C., Snow, R. W., Thiery, W., and van Lipzig, N. P. M.: Can we use local climate zones for predicting malaria prevalence across sub-Saharan African cities?, *Environmental Research Letters*, 15, 124 051, <https://doi.org/10.1088/1748-9326/abc996>, 2020a.
- Brousse, O., Wouters, H., Demuzere, M., Thiery, W., Van de Walle, J., and Lipzig, N. P. M.: The local climate impact of an African city during clear-sky conditions—Implications of the recent urbanization in Kampala (Uganda), *International Journal of Climatology*, 40, 4586–4608, <https://doi.org/10.1002/joc.6477>, 2020b.
- 635 Buchhorn, M., Lesiv, M., Tsendbazar, N. E., Herold, M., Bertels, L., and Smets, B.: Copernicus global land cover layers-collection 2, *Remote Sensing*, 12, 1–14, <https://doi.org/10.3390/rs12061044>, 2020a.
- Buchhorn, M., Smets, B., Bertels, L., Roo, B. D., Lesiv, M., Tsendbazar, N.-E., Herold, M., and Fritz, S.: Copernicus Global Land Service: Land Cover 100m: collection 3: epoch 2018: Globe, <https://doi.org/10.5281/zenodo.3518038>, 2020b.
- 640 Cai, Z., Demuzere, M., Tang, Y., and Wan, Y.: Exploring the characteristics and transformation of 3D urban morphology in three Chinese mega-cities, *Cities* (under review).
- Chen, C., Bagan, H., Xie, X., La, Y., and Yamagata, Y.: Combination of sentinel-2 and palsar-2 for local climate zone classification: A case study of nanchang, China, *Remote Sensing*, 13, 1–21, <https://doi.org/10.3390/rs13101902>, 2021a.



- 645 Chen, G., Xie, J., Li, W., Li, X., Hay Chung, L. C., Ren, C., and Liu, X.: Future “local climate zone” spatial change simulation in Greater Bay Area under the shared socioeconomic pathways and ecological control line, *Building and Environment*, 203, 108077, <https://doi.org/10.1016/j.buildenv.2021.108077>, 2021b.
- Chieppa, J., Bush, A., and Mitra, C.: Using “Local Climate Zones” to detect urban heat island on two small cities in Alabama, *Earth Interactions*, 22, 1–22, <https://doi.org/10.1175/EI-D-17-0020.1>, 2018.
- 650 Chinchor, N.: MUC-4 evaluation metrics, in: *Proceedings of the 4th conference on Message understanding - MUC4 '92*, p. 22, Association for Computational Linguistics, Morristown, NJ, USA, <https://doi.org/10.3115/1072064.1072067>, 1992.
- Ching, J., Mills, G., Bechtel, B., See, L., Feddema, J., Wang, X., Ren, C., Brousse, O., Martilli, A., Neophytou, M., Mouzourides, P., Stewart, I., Hanna, A., Ng, E., Foley, M., Alexander, P., Aliaga, D., Niyogi, D., Shreevastava, A., Bhalachandran, P., Masson, V., Hidalgo, J., Fung, J., Andrade, M., Baklanov, A., Dai, W., Milcinski, G., Demuzere, M., Brunzell, N., Pesaresi, M., Miao, S., Mu, Q., Chen, F., and  
655 Theeuwes, N.: WUDAPT: An Urban Weather, Climate, and Environmental Modeling Infrastructure for the Anthropocene, *Bulletin of the American Meteorological Society*, 99, 1907–1924, <https://doi.org/10.1175/BAMS-D-16-0236.1>, 2018.
- Ching, J., Aliaga, D., Mills, G., Masson, V., See, L., Neophytou, M., Middel, A., Baklanov, A., Ren, C., Ng, E., Fung, J., Wong, M., Huang, Y., Martilli, A., Brousse, O., Stewart, I., Zhang, X., Shehata, A., Miao, S., Wang, X., Wang, W., Yamagata, Y., Duarte, D., Li, Y., Feddema, J., Bechtel, B., Hidalgo, J., Roustan, Y., Kim, Y., Simon, H., Kropp, T., Bruse, M., Lindberg, F., Grimmond, S., Demuzere, M., Chen,  
660 F., Li, C., Gonzales-Cruz, J., Bornstein, B., He, Q., Tzu-Ping, Hanna, A., Erell, E., Tapper, N., Mall, R., and Niyogi, D.: Pathway using WUDAPT’s Digital Synthetic City tool towards generating urban canopy parameters for multi-scale urban atmospheric modeling, *Urban Climate*, 28, 100459, <https://doi.org/10.1016/j.uclim.2019.100459>, 2019.
- Connors, R. W., Trivedi, M. M., and Harlow, C. A.: Segmentation of a high-resolution urban scene using texture operators ( Sunnyvale, California), *Computer Vision, Graphics, & Image Processing*, [https://doi.org/10.1016/0734-189X\(84\)90197-X](https://doi.org/10.1016/0734-189X(84)90197-X), 1984.
- 665 Coops, N. C. and Wulder, M. A.: Breaking the Habit(at), *Trends in Ecology and Evolution*, 34, 585–587, <https://doi.org/10.1016/j.tree.2019.04.013>, 2019.
- Corbane, C., Pesaresi, M., Politis, P., Syrris, V., Florczyk, A. J., Soille, P., Maffenini, L., Burger, A., Vasilev, V., Rodriguez, D., Sabo, F., Dijkstra, L., and Kemper, T.: Big earth data analytics on Sentinel-1 and Landsat imagery in support to global human settlements mapping, *Big Earth Data*, 1, 118–144, <https://doi.org/10.1080/20964471.2017.1397899>, 2017.
- 670 Corbane, C., Politis, P., Kempeneers, P., Simonetti, D., Soille, P., Burger, A., Pesaresi, M., Sabo, F., Syrris, V., and Kemper, T.: A global cloud free pixel- based image composite from Sentinel-2 data, *Data in Brief*, 31, 105737, <https://doi.org/10.1016/j.dib.2020.105737>, 2020.
- Corbane, C., Syrris, V., Sabo, F., Politis, P., Melchiorri, M., Pesaresi, M., Soille, P., and Kemper, T.: Convolutional neural networks for global human settlements mapping from Sentinel-2 satellite imagery, *Neural Computing and Applications*, 33, 6697–6720, <https://doi.org/10.1007/s00521-020-05449-7>, 2021.
- 675 Costello, A., Abbas, M., Allen, A., Ball, S., Bell, S., Bellamy, R., Friel, S., Groce, N., Johnson, A., Kett, M., Lee, M., Levy, C., Maslin, M., McCoy, D., McGuire, B., Montgomery, H., Napier, D., Pagel, C., Patel, J., de Oliveira, J. A. P., Redclift, N., Rees, H., Rogger, D., Scott, J., Stephenson, J., Twigg, J., Wolff, J., and Patterson, C.: Managing the health effects of climate change, *The Lancet*, [https://doi.org/10.1016/s0140-6736\(09\)60935-1](https://doi.org/10.1016/s0140-6736(09)60935-1), 2009.
- Creutzig, F., Baiocchi, G., Bierkandt, R., Pichler, P.-P., and Seto, K. C.: Global typology of urban energy use and potentials for an urbanization  
680 mitigation wedge, *Proceedings of the National Academy of Sciences*, p. 201315545, <https://doi.org/10.1073/pnas.1315545112>, 2015.
- Creutzig, F., Agoston, P., Minx, J. C., Canadell, J. G., Andrew, R. M., Quéré, C. L., Peters, G. P., Sharifi, A., Yamagata, Y., and Dhakal, S.: Urban infrastructure choices structure climate solutions, *Nature Climate Change*, 6, 1054, <https://doi.org/10.1038/nclimate3169>, 2016.



- Creutzig, F., Lohrey, S., Bai, X., Baklanov, A., Dawson, R., Dhakal, S., Lamb, W. F., McPhearson, T., Minx, J., Munoz, E., and Walsh, B.: Upscaling urban data science for global climate solutions, *Global Sustainability*, 2, e2, <https://doi.org/10.1017/sus.2018.16>, 2019.
- 685 D'Amour, C. B., Reitsma, F., Baiocchi, G., Barthel, S., Güneralp, B., Erb, K. H., Haberl, H., Creutzig, F., and Seto, K. C.: Future urban land expansion and implications for global croplands, *Proceedings of the National Academy of Sciences of the United States of America*, 114, 8939–8944, <https://doi.org/10.1073/pnas.1606036114>, 2017.
- Demuzere, M., Orru, K., Heidrich, O., Olazabal, E., Geneletti, D., Orru, H., Bhave, A. G., Mittal, N., Feliu, E., and Faehnle, M.: Mitigating and adapting to climate change: Multi-functional and multi-scale assessment of green urban infrastructure, *Journal of Environmental*  
690 *Management*, 146, 107–115, <https://doi.org/10.1016/j.jenvman.2014.07.025>, 2014.
- Demuzere, M., Bechtel, B., Middel, A., and Mills, G.: Mapping Europe into local climate zones, *PLOS ONE*, 14, e0214474, <https://doi.org/10.1371/journal.pone.0214474>, 2019a.
- Demuzere, M., Bechtel, B., and Mills, G.: Global transferability of local climate zone models, *Urban Climate*, 27, 46–63, <https://doi.org/10.1016/j.uclim.2018.11.001>, 2019b.
- 695 Demuzere, M., Hankey, S., Mills, G., Zhang, W., Lu, T., and Bechtel, B.: Combining expert and crowd-sourced training data to map urban form and functions for the continental US, *Nature Scientific Data*, 7, 1–13, <https://doi.org/10.1038/s41597-020-00605-z>, 2020a.
- Demuzere, M., Mihara, T., Redivo, C. P., Feddema, J., and Setton, E.: Multi-temporal LCZ maps for Canadian functional urban areas, <https://doi.org/10.31219/osf.io/h5tm6>, 2020b.
- Demuzere, M., Argüeso, D., Zonato, A., and Kittner, J.: W2W: A Python package that injects WUDAPT's Local Climate Zone information  
700 in WRF (Version v0.1.1), <https://pypi.org/project/w2w/>, 2021a.
- Demuzere, M., Kittner, J., and Bechtel, B.: LCZ Generator: A Web Application to Create Local Climate Zone Maps, *Frontiers in Environmental Science*, 9, <https://doi.org/10.3389/fenvs.2021.637455>, 2021b.
- Demuzere, M., Kittner, J., Martilli, A., Mills, G., Moede, C., Stewart, I. D., van Vliet, J., and Bechtel, B.: Global map of Local Climate Zones, <https://doi.org/10.5281/zenodo.6364594>, 2022a.
- 705 Demuzere, M., Kittner, J., Martilli, A., Mills, G., Moede, C., Stewart, I. D., van Vliet, J., and Bechtel, B.: Teaser Local Climate Zone maps extracted from the global map of Local Climate Zones, <https://doi.org/10.5281/zenodo.6364705>, 2022b.
- Di Gregorio, A.: Land Cover Classification System Classification concepts and user manual Software version (2), 2005.
- Dunne, J. P., Horowitz, L. W., Adcroft, A. J., Ginoux, P., Held, I. M., John, J. G., Krasting, J. P., Malyshev, S., Naik, V., Paulot, F., Shevliakova, E., Stock, C. A., Zadeh, N., Balaji, V., Blanton, C., Dunne, K. A., Dupuis, C., Durachta, J., Dussin, R., Gauthier, P. P., Griffies, S. M., Guo, H., Hallberg, R. W., Harrison, M., He, J., Hurlin, W., McHugh, C., Menzel, R., Milly, P. C., Nikonov, S., Paynter, D. J., Ploshay, J., Radhakrishnan, A., Rand, K., Reichl, B. G., Robinson, T., Schwarzkopf, D. M., Sentman, L. T., Underwood, S., Vahlenkamp, H., Winton, M., Wittenberg, A. T., Wyman, B., Zeng, Y., and Zhao, M.: The GFDL Earth System Model Version 4.1 (GFDL-ESM 4.1): Overall Coupled Model Description and Simulation Characteristics, *Journal of Advances in Modeling Earth Systems*, 12, 1–56, <https://doi.org/10.1029/2019MS002015>, 2020.
- 715 Eldesoky, A. H., Gil, J., and Pont, M. B.: The suitability of the urban local climate zone classification scheme for surface temperature studies in distinct macroclimate regions, *Urban Climate*, 37, 100823, <https://doi.org/10.1016/j.uclim.2021.100823>, 2021.
- ESA: Land Cover CCI Product User Guide Version 2.0, Tech. rep., European Space Agency, 2017.
- Esch, T., Heldens, W., Hirne, A., Keil, M., Marconcini, M., Roth, A., Zeidler, J., Dech, S., and Strano, E.: Breaking new ground in mapping human settlements from space -The Global Urban Footprint-, *ISPRS Journal of Photogrammetry and Remote Sensing*, 134, 30–42,  
720 <https://doi.org/10.1016/j.isprsjprs.2017.10.012>, 2017.



- European Environment Agency: Copernicus Land Monitoring Service - High Resolution Layers - Imperviousness Density, <https://land.copernicus.eu/pan-european/high-resolution-layers/imperviousness/status-maps/imperviousness-density-2018>, 2018a.
- European Environment Agency: Copernicus Land Monitoring Service - High Resolution Layers - Impervious Built-up, <https://land.copernicus.eu/pan-european/high-resolution-layers/imperviousness/status-maps/impervious-built-up-2018>, 2018b.
- 725 Fenner, D., Meier, F., Bechtel, B., Otto, M., and Scherer, D.: Intra and inter ‘local climate zone’ variability of air temperature as observed by crowdsourced citizen weather stations in Berlin, Germany, *Meteorologische Zeitschrift*, 26, 525–547, <https://doi.org/10.1127/metz/2017/0861>, 2017.
- Fenner, D., Bechtel, B., Demuzere, M., Kittner, J., and Meier, F.: CrowdQC+—A Quality-Control for Crowdsourced Air-Temperature Observations Enabling World-Wide Urban Climate Applications, *Frontiers in Environmental Science*, 9, 1–21, <https://doi.org/10.3389/fenvs.2021.720747>, 2021.
- 730 Florczyk, A., Melchiorri, M., Corban, C., Schiavina, M., Maffenini, L., Pesaresi, M., Politis, P., Sabo, F., Carneiro Freire, S., Ehrlich, D., Kemper, T., Tommasi, P., Airaghi, D., and Zanchetta, L.: Description of the GHS Urban Centre Database 2015, <https://doi.org/10.2760/037310> (online), 2019.
- Forget, Y., Shimoni, M., and Gilbert, M.: Complementarity Between Sentinel-1 and Landsat 8 Imagery for Built-Up Mapping in Sub-Saharan Africa, pp. 1–13, <https://doi.org/10.20944/preprints201810.0695.v1>, 2018.
- 735 Fuhrer, O., Chadha, T., Hoefler, T., Kwasniewski, G., Lapillonne, X., Leutwyler, D., Lüthi, D., Osuna, C., Schär, C., Schulthess, T. C., and Vogt, H.: Near-global climate simulation at 1km resolution: Establishing a performance baseline on 4888 GPUs with COSMO 5.0, *Geoscientific Model Development*, 11, 1665–1681, <https://doi.org/10.5194/gmd-11-1665-2018>, 2018.
- Gál, T., Mahó, S. I., Skarbit, N., and Unger, J.: Numerical modelling for analysis of the effect of different urban green spaces on urban heat load patterns in the present and in the future, *Computers, Environment and Urban Systems*, 87, <https://doi.org/10.1016/j.compenvurbsys.2021.101600>, 2021.
- 740 Georgescu, M., Chow, W. T. L., Wang, Z. H., Brazel, a., Trapido-Lurie, B., Roth, M., and Benson-Lira, V.: Prioritizing urban sustainability solutions: coordinated approaches must incorporate scale-dependent built environment induced effects, *Environmental Research Letters*, 10, 061 001, <https://doi.org/10.1088/1748-9326/10/6/061001>, 2015.
- 745 Gilabert, J., Deluca, A., Lauwaet, D., Ballester, J., Corbera, J., and Llasat, M. C.: Assessing heat exposure to extreme temperatures in urban areas using the Local Climate Zones classification, *Natural Hazards and Earth System Sciences Discussions*, pp. 1–41, <https://doi.org/10.5194/nhess-2020-240>, 2020.
- Gong, P., Li, X., Wang, J., Bai, Y., Chen, B., Hu, T., Liu, X., Xu, B., Yang, J., Zhang, W., and Zhou, Y.: Annual maps of global artificial impervious area (GAIA) between 1985 and 2018, *Remote Sensing of Environment*, 236, 111 510, <https://doi.org/10.1016/j.rse.2019.111510>, 2020.
- 750 Gorelick, N., Hancher, M., Dixon, M., Ilyushchenko, S., Thau, D., and Moore, R.: Google Earth Engine: Planetary-scale geospatial analysis for everyone, *Remote Sensing of Environment*, 202, 18–27, <https://doi.org/10.1016/j.rse.2017.06.031>, 2017.
- Grimm, N. B., Faeth, S. H., Golubiewski, N. E., Redman, C. L., Wu, J., Bai, X., and Briggs, J. M.: Global change and the ecology of cities., *Science (New York, N.Y.)*, 319, 756–760, <https://doi.org/10.1126/science.1150195>, 2008.
- 755 Grimmond, S., Bouchet, V., Molina, L. T., Baklanov, A., Tan, J., Schlünzen, K. H., Mills, G., Golding, B., Masson, V., Ren, C., Voogt, J., Miao, S., Lean, H., Heusinkveld, B., Hovespyan, A., Teruggi, G., Parrish, P., and Joe, P.: Integrated urban hydrometeorological, climate and environmental services: Concept, methodology and key messages, *Urban Climate*, 33, 100 623, <https://doi.org/10.1016/j.uclim.2020.100623>, 2020.



- Güneralp, B., Zhou, Y., Ürge-Vorsatz, D., Gupta, M., Yu, S., Patel, P. L., Fragkias, M., Li, X., and Seto, K. C.: Global scenarios of urban density and its impacts on building energy use through 2050, *Proceedings of the National Academy of Sciences of the United States of America*, 114, 8945–8950, <https://doi.org/10.1073/pnas.1606035114>, 2017.
- Gutowski, W. J., Ullrich, P. A., Hall, A., Leung, L. R., O'Brien, T. A., Patricola, C. M., Arritt, R. W., Bukovsky, M. S., Calvin, K. V., Feng, Z., Jones, A. D., Kooperman, G. J., Monier, E., Pritchard, M. S., Pryor, S. C., Qian, Y., Rhoades, A. M., Roberts, A. F., Sakaguchi, K., Urban, N., and Zarzycki, C.: The Ongoing Need for High-Resolution Regional Climate Models: Process Understanding and Stakeholder Information, *Bulletin of the American Meteorological Society*, 101, E664–E683, <https://doi.org/10.1175/BAMS-D-19-0113.1>, 2020.
- Hammerberg, K., Brousse, O., Martilli, A., and Mahdavi, A.: Implications of employing detailed urban canopy parameters for mesoscale climate modelling: a comparison between WUDAPT and GIS databases over Vienna, Austria, *International Journal of Climatology*, 38, e1241–e1257, <https://doi.org/10.1002/joc.5447>, 2018.
- Haralick, R. M., Dinstein, I., and Shanmugam, K.: Textural Features for Image Classification, *IEEE Transactions on Systems, Man and Cybernetics*, <https://doi.org/10.1109/TSMC.1973.4309314>, 1973.
- Hay Chung, L. C., Xie, J., and Ren, C.: Improved machine-learning mapping of local climate zones in metropolitan areas using composite Earth observation data in Google Earth Engine, *Building and Environment*, 199, 107 879, <https://doi.org/10.1016/j.buildenv.2021.107879>, 2021.
- Hertwig, D., Ng, M., Grimmond, S., Vidale, P. L., and McGuire, P. C.: High-resolution global climate simulations: Representation of cities, *International Journal of Climatology*, 41, 3266–3285, <https://doi.org/10.1002/joc.7018>, 2021.
- Hidalgo, J., Lemonsu, A., and Masson, V.: Between progress and obstacles in urban climate interdisciplinary studies and knowledge transfer to society, *Annals of the New York Academy of Sciences*, pp. 1–14, <https://doi.org/10.1111/nyas.13986>, 2018.
- Hirsch, A. L., Evans, J. P., Thomas, C., Conroy, B., Hart, M. A., Lipson, M., and Ertler, W.: Resolving the influence of local flows on urban heat amplification during heatwaves, *Environmental Research Letters*, 16, 064 066, <https://doi.org/10.1088/1748-9326/ac0377>, 2021.
- Hu, J., Ghamisi, P., and Zhu, X.: Feature Extraction and Selection of Sentinel-1 Dual-Pol Data for Global-Scale Local Climate Zone Classification, *ISPRS International Journal of Geo-Information*, 7, 379, <https://doi.org/10.3390/ijgi7090379>, 2018.
- IPCC: *Climate Change 2022: Impacts, Adaptation, and Vulnerability. Contribution of Working Group II to the Sixth Assessment Report of the Intergovernmental Panel on Climate Change*, 2022.
- Jiang, S., Huang, F., Zhan, W., Bechtel, B., Liu, Z., Demuzere, M., Huang, Y., Xu, Y., Xia, W., Quan, J., Hong, F., Jiang, L., Lai, J., Wang, C., Kong, F., Du, H., Miao, S., Chen, Y., Zhang, X., Planning, R., and Development, U.: Mapping Local Climate Zones : A Bibliometric Meta- Analysis and Systematic Review, *OSF preprints*, pp. 1–106, <https://doi.org/10.31219/osf.io/c2bez>, 2021.
- Jung, M., Dahal, P. R., Butchart, S. H., Donald, P. F., De Lamo, X., Lesiv, M., Kapos, V., Rondinini, C., and Visconti, P.: A global map of terrestrial habitat types, *Scientific Data*, 7, 1–8, <https://doi.org/10.1038/s41597-020-00599-8>, 2020.
- Kabano, P., Lindley, S., and Harris, A.: Evidence of urban heat island impacts on the vegetation growing season length in a tropical city, *Landscape and Urban Planning*, 206, 103 989, <https://doi.org/10.1016/j.landurbplan.2020.103989>, 2021.
- Karsisto, P., Fortelius, C., Demuzere, M., Grimmond, C. S. B., Oleson, K. W., Kouznetsov, R., Masson, V., and Järvi, L.: Seasonal surface urban energy balance and wintertime stability simulated using three land-surface models in the high-latitude city Helsinki, *Quarterly Journal of the Royal Meteorological Society*, 142, 401–417, <https://doi.org/10.1002/qj.2659>, 2016.
- Kotharkar, R., Ghosh, A., Kapoor, S., and Reddy, D. G. K.: Approach to local climate zone based energy consumption assessment in an Indian city, *Energy and Buildings*, p. 111835, <https://doi.org/10.1016/j.enbuild.2022.111835>, 2022.



- Kuffer, M., Thomson, D. R., Boo, G., Mahabir, R., Grippa, T., Vanhuyse, S., Engstrom, R., Ndugwa, R., Makau, J., Darin, E., de Albuquerque, J. P., and Kabaria, C.: The role of earth observation in an integrated deprived area mapping "system" for low-to-middle income countries, *Remote Sensing*, 12, <https://doi.org/10.3390/rs12060982>, 2020.
- Lai, D., Liu, W., Gan, T., Liu, K., and Chen, Q.: A review of mitigating strategies to improve the thermal environment and thermal comfort  
800 in urban outdoor spaces, *Science of the Total Environment*, 661, 337–353, <https://doi.org/10.1016/j.scitotenv.2019.01.062>, 2019.
- Leconte, F., Bouyer, J., and Claverie, R.: Nocturnal cooling in Local Climate Zone: Statistical approach using mobile measurements, *Urban Climate*, 33, 100 629, <https://doi.org/10.1016/j.uclim.2020.100629>, 2020.
- Lehnert, M., Savić, S., Milošević, D., Dunjić, J., and Geletič, J.: Mapping Local Climate Zones and Their Applications in European Urban Environments: A Systematic Literature Review and Future Development Trends, *ISPRS International Journal of Geo-Information*, 10,  
805 260, <https://doi.org/10.3390/ijgi10040260>, 2021.
- Li, M., Koks, E., Taubenböck, H., and van Vliet, J.: Continental-scale mapping and analysis of 3D building structure, *Remote Sensing of Environment*, 245, 111 859, <https://doi.org/10.1016/j.rse.2020.111859>, 2020a.
- Li, X., Gong, P., Zhou, Y., Wang, J., Bai, Y., Chen, B., Hu, T., Xiao, Y., Xu, B., Yang, J., Liu, X., Cai, W., Huang, H., Wu, T., Wang, X., Lin, P., Li, X., Chen, J., He, C., Li, X., Yu, L., Clinton, N., and Zhu, Z.: Mapping global urban boundaries from the global artificial impervious  
810 area (GAIA) data, *Environmental Research Letters*, 15, <https://doi.org/10.1088/1748-9326/ab9be3>, 2020b.
- Lindberg, F., Grimmond, C., Gabey, A., Huang, B., Kent, C. W., Sun, T., Theeuwes, N. E., Järvi, L., Ward, H. C., Capel-Timms, I., Chang, Y., Jonsson, P., Krave, N., Liu, D., Meyer, D., Olofson, K. F. G., Tan, J., Wästberg, D., Xue, L., and Zhang, Z.: Urban Multi-scale Environmental Predictor (UMEP): An integrated tool for city-based climate services, *Environmental Modelling & Software*, 99, 70–87, <https://doi.org/10.1016/j.envsoft.2017.09.020>, 2018.
- 815 Liu, S., Qi, Z., Li, X., and Yeh, A. G.-o.: Integration of Convolutional Neural Networks and Object-Based Post-Classification Refinement for Land Use and Land Cover Mapping with Optical and SAR Data, pp. 1–25, <https://doi.org/10.3390/rs11060690>, 2019.
- Lu, T., Marshall, J. D., Zhang, W., Hystad, P., Kim, S.-Y., Bechle, M. J., Demuzere, M., and Hankey, S.: National Empirical Models of Air Pollution Using Microscale Measures of the Urban Environment, *Environmental Science & Technology*, <https://doi.org/10.1021/acs.est.1c04047>, 2021a.
- 820 Lu, Y., Yang, J., and Ma, S.: Dynamic Changes of Local Climate Zones in the Guangdong–Hong Kong–Macao Greater Bay Area and Their Spatio-Temporal Impacts on the Surface Urban Heat Island Effect between 2005 and 2015, *Sustainability*, 13, 6374, <https://doi.org/10.3390/su13116374>, 2021b.
- Lyu, T., Buccolieri, R., and Gao, Z.: A numerical study on the correlation between sky view factor and summer microclimate of local climate zones, *Atmosphere*, 10, <https://doi.org/10.3390/atmos10080438>, 2019.
- 825 MacKenzie, A. R., Whyatt, J. D., Barnes, M. J., Davies, G., and Hewitt, C. N.: Urban form strongly mediates the allometric scaling of airshed pollution concentrations, *Environmental Research Letters*, 14, <https://doi.org/10.1088/1748-9326/ab50e3>, 2019.
- Maharroof, N., Emmanuel, R., and Thomson, C.: Compatibility of local climate zone parameters for climate sensitive street design: Influence of openness and surface properties on local climate, *Urban Climate*, 33, 100 642, <https://doi.org/10.1016/j.uclim.2020.100642>, 2020.
- Manoli, G., Faticchi, S., Schläpfer, M., Yu, K., Crowther, T. W., Meili, N., Burlando, P., Katul, G. G., and Bou-Zeid, E.: Magnitude of urban  
830 heat islands largely explained by climate and population, *Nature*, 573, 55–60, <https://doi.org/10.1038/s41586-019-1512-9>, 2019.
- Marconcini, M., Metz-Marconcini, A., Üreyen, S., Palacios-Lopez, D., Hanke, W., Bachofer, F., Zeidler, J., Esch, T., and Strano, E.: World Settlement Footprint (WSF) 2015 - Percent Settlement Area - 100m, Figshare, <https://doi.org/10.6084/m9.figshare.10048475.v1>, 2020.



- Martilli, A.: An idealized study of city structure, urban climate, energy consumption, and air quality, *Urban Climate*, 10, 430–446, <https://doi.org/10.1016/j.uclim.2014.03.003>, 2014.
- 835 Martilli, A., Roth, M., Winston, T. L., Demuzere, M., Lipson, M., Krayenhoff, S., Sailor, D., Nazarian, N., Voogt, J., Wouters, H., Middel, A., Stewart, I. D., Bechtel, B., Christen, A., and Hart, M.: Summer average urban-rural surface temperature differences do not indicate the need for urban heat reduction, OSF preprints, <https://doi.org/10.31219/osf.io/8gnbf>, 2020.
- Masson, V., Heldens, W., Bocher, E., Bonhomme, M., Bucher, B., Burmeister, C., de Munck, C., Esch, T., Hidalgo, J., Kanani-Sühring, F., Kwok, Y. T., Lemonsu, A., Lévy, J. P., Maronga, B., Pavlik, D., Petit, G., See, L., Schoetter, R., Tornay, N., Votsis, A., and Zeidler, J.: City-descriptive input data for urban climate models: Model requirements, data sources and challenges, *Urban Climate*, 31, 100536, <https://doi.org/10.1016/j.uclim.2019.100536>, 2020.
- 840 Matsaba, E. O., Langer, I., Adimo, A. O., Mukundi, J. B., and Wesonga, J. M.: Spatio-Temporal Variability of Simulated 2 m Air Temperature for Nairobi City, Kenya, *Current Urban Studies*, 08, 205–221, <https://doi.org/10.4236/cus.2020.82011>, 2020.
- McDonough, L. K., Santos, I. R., Andersen, M. S., O’Carroll, D. M., Rutledge, H., Meredith, K., Oudone, P., Bridgeman, J., Goody, D. C., Sorensen, J. P., Lapworth, D. J., MacDonald, A. M., Ward, J., and Baker, A.: Changes in global groundwater organic carbon driven by climate change and urbanization, *Nature Communications*, 11, 1–10, <https://doi.org/10.1038/s41467-020-14946-1>, 2020.
- 845 Middel, A., Häb, K., Brazel, A. J., Martin, C. a., and Guhathakurta, S.: Impact of urban form and design on mid-afternoon microclimate in Phoenix Local Climate Zones, *Landscape and Urban Planning*, 122, 16–28, <https://doi.org/10.1016/j.landurbplan.2013.11.004>, 2014.
- Mills, S., Weiss, S., and Liang, C.: VIIRS day/night band (DNB) stray light characterization and correction, in: *Earth Observing Systems XVIII*, edited by Butler, J. J., Xiong, X. J., and Gu, X., vol. 8866, pp. 549–566, International Society for Optics and Photonics, SPIE, <https://doi.org/10.1117/12.2023107>, 2013.
- 850 Milošević, D., Savić, S., Kresoja, M., Lužanin, Z., Šećerov, I., Arsenović, D., Dunjić, J., and Matzarakis, A.: Analysis of air temperature dynamics in the “local climate zones” of Novi Sad (Serbia) based on long-term database from an urban meteorological network, *International Journal of Biometeorology*, <https://doi.org/10.1007/s00484-020-02058-w>, 2021.
- 855 Molnár, G., Gyöngyösi, A. Z., and Gál, T.: Integration of an LCZ-based classification into WRF to assess the intra-urban temperature pattern under a heatwave period in Szeged, Hungary, *Theoretical and Applied Climatology*, 138, 1139–1158, <https://doi.org/10.1007/s00704-019-02881-1>, 2019.
- Moradi, M., Krayenhoff, E. S., and Aliabadi, A. A.: A comprehensive indoor–outdoor urban climate model with hydrology: The Vertical City Weather Generator (VCWG v2.0.0), *Building and Environment*, 207, 108406, <https://doi.org/10.1016/j.buildenv.2021.108406>, 2022.
- 860 Mu, Q., Miao, S., Wang, Y., Li, Y., He, X., and Yan, C.: Evaluation of employing local climate zone classification for mesoscale modelling over Beijing metropolitan area, *Meteorology and Atmospheric Physics*, 132, 315–326, <https://doi.org/10.1007/s00703-019-00692-7>, 2020.
- Nagendra, H., Bai, X., Brondizio, E. S., and Lwasa, S.: The urban south and the predicament of global sustainability, *Nature Sustainability*, 1, 341–349, <https://doi.org/10.1038/s41893-018-0101-5>, 2018.
- Oke, T. R., Mills, G., Christen, A., and Voogt, J. A.: *Urban Climates*, Cambridge University Press, Cambridge, <https://doi.org/10.1017/9781139016476>, 2017.
- 865 Oleson, K. W. and Feddema, J.: Parameterization and Surface Data Improvements and New Capabilities for the Community Land Model Urban (CLMU), *Journal of Advances in Modeling Earth Systems*, 12, 1–30, <https://doi.org/10.1029/2018ms001586>, 2020.
- Owusu, M., Kuffer, M., Belgiu, M., Grippa, T., Lennert, M., Georganos, S., and Vanhuysse, S.: Towards user-driven earth observation-based slum mapping, *Computers, Environment and Urban Systems*, 89, 101681, <https://doi.org/10.1016/j.compenvurbsys.2021.101681>, 2021.



- 870 Pan, Z.: WUDAPT Level 0 training data for HUAICHU (China, People's Republic of), submitted to the LCZ Generator. This dataset is licensed under CC BY-SA, and more information is available at [https://lcz-generator.rub.de/factsheets/f81f240993b6ca50180232c878755c18736e308a/f81f240993b6ca50180232c878755c18736e308a\\_factsheet.html](https://lcz-generator.rub.de/factsheets/f81f240993b6ca50180232c878755c18736e308a/f81f240993b6ca50180232c878755c18736e308a_factsheet.html), 2021.
- Patel, P., Karmakar, S., Ghosh, S., and Niyogi, D.: Improved simulation of very heavy rainfall events by incorporating WUDAPT urban land use/land cover in WRF, *Urban Climate*, 32, 100 616, <https://doi.org/10.1016/j.uclim.2020.100616>, 2020.
- 875 Patel, P., Jamshidi, S., Nadimpalli, R., Aliaga, D. G., Mills, G., Chen, F., Demuzere, M., and Niyogi, D.: Modeling Large-Scale Heatwave by Incorporating Enhanced Urban Representation, *Journal of Geophysical Research: Atmospheres*, 127, 1–33, <https://doi.org/10.1029/2021JD035316>, 2022.
- Patella, V., Florio, G., Magliacane, D., Giuliano, A., Crivellaro, M. A., Bartolomeo, D., Genovese, A., Palmieri, M., Postiglione, A., Ridolo, E., Scaletti, C., Ventura, M. T., and Zollo, A.: Urban air pollution and climate change: "The Decalogue: Allergy Safe Tree" for allergic and respiratory diseases care, *Clinical and Molecular Allergy*, 16, 1, <https://doi.org/10.1186/s12948-018-0098-3>, 2018.
- 880 Pedregosa, F., Varoquaux, G., Gramfort, A., Michel, V., Thirion, B., Grisel, O., Blondel, M., Prettenhofer, P., Weiss, R., Dubourg, V., Vanderplas, J., Passos, A., Cournapeau, D., Brucher, M., Perrot, M., and Duchesnay, E.: Scikit-learn: Machine Learning in {P}ython, *Journal of Machine Learning Research*, 12, 2825–2830, 2011.
- Pellegatti Franco, D. M., Andrade, M. d. F., Ynoue, R. Y., and Ching, J.: Effect of Local Climate Zone (LCZ) classification on ozone chemical transport model simulations in Sao Paulo, Brazil, *Urban Climate*, 27, 293–313, <https://doi.org/10.1016/j.uclim.2018.12.007>, 2019.
- 885 Perera, N. and Emmanuel, R.: A "Local Climate Zone" based approach to urban planning in Colombo, Sri Lanka, *Urban Climate*, 23, 188–203, <https://doi.org/10.1016/j.uclim.2016.11.006>, 2018.
- Potapov, P., Li, X., Hernandez-Serna, A., Tyukavina, A., Hansen, M. C., Kommareddy, A., Pickens, A., Turubanova, S., Tang, H., Silva, C. E., Armston, J., Dubayah, R., Blair, J. B., and Hofton, M.: Mapping global forest canopy height through integration of GEDI and Landsat data, *Remote Sensing of Environment*, 253, 112 165, <https://doi.org/10.1016/j.rse.2020.112165>, 2021.
- 890 Quah, A. K. and Roth, M.: Diurnal and weekly variation of anthropogenic heat emissions in a tropical city, Singapore, *Atmospheric Environment*, 46, 92–103, <https://doi.org/10.1016/j.atmosenv.2011.10.015>, 2012.
- Raven, J., Stone, B., Mills, G., Towers, J., Katzschner, L., Leone, M. F., Gaborit, P., Georgescu, M., Hariri, M., Lee, J., Le-Java, J., Sharifi, A., Visconti, C., and Rudd, A.: Urban Planning and Urban Design, *Climate Change and Cities*, pp. 139–172, <https://doi.org/10.1017/9781316563878.012>, 2018.
- 895 Reba, M. and Seto, K. C.: A systematic review and assessment of algorithms to detect, characterize, and monitor urban land change, *Remote Sensing of Environment*, 242, 111 739, <https://doi.org/10.1016/j.rse.2020.111739>, 2020.
- Ribeiro, H. V., Rybski, D., and Kropp, J. P.: Effects of changing population or density on urban carbon dioxide emissions, *Nature Communications*, 10, 1–9, <https://doi.org/10.1038/s41467-019-11184-y>, 2019.
- 900 Rosentreter, J., Hagensieker, R., and Waske, B.: Towards large-scale mapping of local climate zones using multitemporal Sentinel 2 data and convolutional neural networks, *Remote Sensing of Environment*, 237, 111 472, <https://doi.org/10.1016/j.rse.2019.111472>, 2020.
- Rosenzweig, C., Solecki, W., Hammer, S. a., and Mehrotra, S.: Cities lead the way in climate-change action., *Nature*, 467, 909–911, <https://doi.org/10.1038/467909a>, 2010.
- Santos, L. G. R., Singh, V. K., Mughal, M. O., Nevat, I., Norford, L. K., and Fonseca, J. A.: Estimating building's anthropogenic heat: a joint local climate zone and land use classification method, in: eSIM 2021 conference, pp. 12–19, <https://doi.org/10.3929/ethz-b-000445814>, 2020.
- 905



- Sapena, M., Wurm, M., Taubenböck, H., Tuia, D., and Ruiz, L. A.: Estimating quality of life dimensions from urban spatial pattern metrics, *Computers, Environment and Urban Systems*, 85, <https://doi.org/10.1016/j.compenvurbsys.2020.101549>, 2021.
- Schär, C., Fuhrer, O., Arteaga, A., Ban, N., Charpillot, C., Di Girolamo, S., Hentgen, L., Hoefler, T., Lapillonne, X., Leutwyler, D., Osterried, K., Panosetti, D., Rüdüsühli, S., Schlemmer, L., Schulthess, T. C., Sprenger, M., Ubbiali, S., and Wernli, H.: Kilometer-Scale Climate Models: Prospects and Challenges, *Bulletin of the American Meteorological Society*, 101, E567–E587, <https://doi.org/10.1175/bams-d-18-0167.1>, 2020.
- Schiavina, M., Moreno-Monroy, A., Maffenini, L., and Veneri, P.: GHSL-OECD Functional Urban Areas 2019, <https://doi.org/10.2760/67415>, 2019.
- Schlöpfer, M., Lee, J., and Bettencourt, L. M. A.: Urban Skylines: building heights and shapes as measures of city size, pp. 1–17, <http://arxiv.org/abs/1512.00946>, 2015.
- Schneider, A., Friedl, M. a., and Potere, D.: Mapping global urban areas using MODIS 500-m data: New methods and datasets based on ‘urban ecoregions’, *Remote Sensing of Environment*, 114, 1733–1746, <https://doi.org/10.1016/j.rse.2010.03.003>, 2010.
- Seto, K. C., Güneralp, B., and Hutyra, L. R.: Global forecasts of urban expansion to 2030 and direct impacts on biodiversity and carbon pools., *Proceedings of the National Academy of Sciences of the United States of America*, 109, 16083–8, <https://doi.org/10.1073/pnas.1211658109>, 2012.
- Sharma, R., Hooyberghs, H., Lauwaet, D., and De Ridder, K.: Urban Heat Island and Future Climate Change—Implications for Delhi’s Heat, *Journal of Urban Health*, 96, 235–251, <https://doi.org/10.1007/s11524-018-0322-y>, 2019.
- Shimada, M., Itoh, T., Motooka, T., Watanabe, M., Shiraishi, T., Thapa, R., and Lucas, R.: New global forest/non-forest maps from ALOS PALSAR data (2007–2010), *Remote Sensing of Environment*, 155, 13–31, <https://doi.org/10.1016/j.rse.2014.04.014>, 2014.
- Simard, M., Pinto, N., Fisher, J. B., and Baccini, A.: Mapping forest canopy height globally with spaceborne lidar, *Journal of Geophysical Research*, 116, G04021, <https://doi.org/10.1029/2011JG001708>, 2011.
- Skarbit, N., Stewart, I. D., Unger, J., and Gál, T.: Employing an urban meteorological network to monitor air temperature conditions in the ‘local climate zones’ of Szeged, Hungary, *International Journal of Climatology*, 37, 582–596, <https://doi.org/10.1002/joc.5023>, 2017.
- Steenefeld, G.-J., Klomp maker, J. O., Groen, R. J., and Holtslag, A. A.: An urban climate assessment and management tool for combined heat and air quality judgements at neighbourhood scales, *Resources, Conservation and Recycling*, 132, 204–217, <https://doi.org/10.1016/j.resconrec.2016.12.002>, 2018.
- Stewart, I. D.: A systematic review and scientific critique of methodology in modern urban heat island literature, *International Journal of Climatology*, 31, 200–217, <https://doi.org/10.1002/joc.2141>, 2011a.
- Stewart, I. D.: Redefining the Urban Heat Island, pp. 1–352, <https://circle.ubc.ca/handle/2429/38069>, 2011b.
- Stewart, I. D.: Developing a field guide to identify ‘local climate zones’ in cities, in: 10th International Conference on Urban Climate / 14th Symposium on the Urban Environment, New York City, USA, 2018.
- Stewart, I. D. and Mills, G.: The Urban Heat Island - A Guidebook, Elsevier, <https://doi.org/10.1016/C2017-0-02872-0>, 2021.
- Stewart, I. D. and Oke, T. R.: Local Climate Zones for Urban Temperature Studies, *Bulletin of the American Meteorological Society*, 93, 1879–1900, <https://doi.org/10.1175/BAMS-D-11-00019.1>, 2012.
- Stewart, I. D., Krayenhoff, E. S., Voogt, J. A., Lachapelle, J. A., Allen, M. A., and Broadbent, A. M.: Time Evolution of the Surface Urban Heat Island, *Earth’s Future*, 9, <https://doi.org/10.1029/2021EF002178>, 2021.
- Stone, B., Mednick, A. C., Holloway, T., and Spak, S. N.: Is Compact Growth Good for Air Quality?, *Journal of the American Planning Association*, 73, 404–418, <https://doi.org/10.1080/01944360708978521>, 2007.



- 945 Tadono, T., Nagai, H., Ishida, H., Oda, F., Naito, S., Minakawa, K., and Iwamoto, H.: Generation of the 30 M-MESH global digital surface model by alos prism, in: International Archives of the Photogrammetry, Remote Sensing and Spatial Information Sciences - ISPRS Archives, pp. 157–162, <https://doi.org/10.5194/isprsarchives-XLI-B4-157-2016>, 2016.
- Takane, Y., Kikegawa, Y., Hara, M., and Grimmond, C. S. B.: Urban warming and future air-conditioning use in an Asian megacity: importance of positive feedback, *npj Climate and Atmospheric Science*, 2, 1–11, <https://doi.org/10.1038/s41612-019-0096-2>, 2019.
- 950 Taubenböck, H., Debray, H., Qiu, C., Schmitt, M., Wang, Y., and Zhu, X. X.: Seven city types representing morphologic configurations of cities across the globe, *Cities*, 105, 102 814, <https://doi.org/10.1016/j.cities.2020.102814>, 2020.
- UN: World Urbanization Prospects: The 2018 Revision, Population Division of the United Nations Department of Economic and Social Affairs, <https://doi.org/10.18356/b9e995fe-en>, 2019.
- Van de Walle, J., Brousse, O., Arnalsteen, L., Byarugaba, D., Ddumba, D. S., Demuzere, M., Lwasa, S., Nsangi, G., Sseviiri, H., Thiery, W.,  
955 Vanhaeren, R., Wouters, H., and P.M. van Lipzig, N.: Can local fieldwork help to represent intra-urban variability of canopy parameters relevant for tropical African climate studies?, *Theoretical and Applied Climatology*, <https://doi.org/10.1007/s00704-021-03733-7>, 2021.
- Van de Walle, J., Brousse, O., Arnalsteen, L., Brimicombe, C., Byarugaba, D., Demuzere, M., Jjemba, E., Lwasa, S., Misiani, H., Nsangi, G., Soetewey, F., Sseviiri, H., Thiery, W., Vanhaeren, R., Zaitchik, B. F., and van Lipzig, N. P. M.: Lack of vegetation exacerbates exposure to dangerous heat in dense settlements in a tropical African city, *Environmental Research Letters*, 17, 024 004, <https://doi.org/10.1088/1748-9326/ac47c3>, 2022.
- 960 van Vliet, J.: Direct and indirect loss of natural area from urban expansion, *Nature Sustainability*, 2, 755–763, <https://doi.org/10.1038/s41893-019-0340-0>, 2019.
- Vandamme, S., Demuzere, M., Verdonck, M.-l., Zhang, Z., and Coillie, F. V.: Revealing Kunming’s (China) Historical Urban Planning Policies Through Local Climate Zones, *Remote Sensing*, 11, 1731, <https://doi.org/10.3390/rs11141731>, 2019.
- 965 Varentsov, M., Samsonov, T., and Demuzere, M.: Impact of Urban Canopy Parameters on a Megacity’s Modelled Thermal Environment, *Atmosphere*, 11, 1349, <https://doi.org/10.3390/atmos11121349>, 2020.
- Varentsov, M., Fenner, D., Meier, F., and Samsonov, T.: Quantifying Local and Mesoscale Drivers of the Urban Heat Island of Moscow with Reference and Crowdsourced Observations, *Frontiers in Environmental Science*, 9, 1–21, <https://doi.org/10.3389/fenvs.2021.716968>, 2021.
- 970 Varquez, A. C., Shota, K., Khanh, D. N., and Kanda, M.: Global 1-km present and future hourly anthropogenic heat flux, Figshare, <https://doi.org/10.6084/m9.figshare.12612458.v6>, 2020.
- Varquez, A. C. G., Kiyomoto, S., Khanh, D. N., and Kanda, M.: Global 1-km present and future hourly anthropogenic heat flux, *Scientific Data*, 8, 64, <https://doi.org/10.1038/s41597-021-00850-w>, 2021.
- Verdonck, M.-L., Okujeni, A., van der Linden, S., Demuzere, M., De Wulf, R., and Van Coillie, F.: Influence of neighbourhood information  
975 on ‘Local Climate Zone’ mapping in heterogeneous cities, *International Journal of Applied Earth Observation and Geoinformation*, 62, <https://doi.org/10.1016/j.jag.2017.05.017>, 2017.
- Verdonck, M.-l., Demuzere, M., Hooyberghs, H., Beck, C., Cyrus, J., Schneider, A., Dewulf, R., and Van Coillie, F.: The potential of local climate zones maps as a heat stress assessment tool, supported by simulated air temperature data, *Landscape and Urban Planning*, 178, 183–197, <https://doi.org/10.1016/j.landurbplan.2018.06.004>, 2018.
- 980 Verdonck, M.-l., Demuzere, M., Bechtel, B., Beck, C., Brousse, O., Droste, A., Fenner, D., Leconte, F., and Van Coillie, F.: The Human Influence Experiment (Part 2): Guidelines for Improved Mapping of Local Climate Zones Using a Supervised Classification, *Urban Science*, 3, 27, <https://doi.org/10.3390/urbansci3010027>, 2019a.



- Verdonck, M.-L., Demuzere, M., Hooyberghs, H., Priem, F., and Van Coillie, F.: Heat risk assessment for the Brussels capital region under different urban planning and greenhouse gas emission scenarios, *Journal of Environmental Management*, 249, 109 210, 985 <https://doi.org/10.1016/j.jenvman.2019.06.111>, 2019b.
- Wang, J. and Ouyang, W.: Attenuating the surface Urban Heat Island within the Local Thermal Zones through land surface modification, *Journal of Environmental Management*, 187, 239–252, <https://doi.org/10.1016/j.jenvman.2016.11.059>, 2017.
- Wang, J., Chen, Y., Liao, W., He, G., Tett, S. F. B., Yan, Z., Zhai, P., Feng, J., Ma, W., Huang, C., and Hu, Y.: Anthropogenic emissions and urbanization increase risk of compound hot extremes in cities, *Nature Climate Change*, 11, 1084–1089, <https://doi.org/10.1038/s41558-021-01196-2>, 2021. 990
- Wang, R., Cai, M., Ren, C., Bechtel, B., Xu, Y., and Ng, E.: Detecting multi-temporal land cover change and land surface temperature in Pearl River Delta by adopting local climate zone, *Urban Climate*, 28, 100 455, <https://doi.org/10.1016/j.uclim.2019.100455>, 2019.
- Williams, K., Joynt, J. L., and Hopkins, D.: Adapting to Climate Change in the Compact City: The Suburban Challenge, *Built Environment*, 36, 105–115, <https://doi.org/10.2148/benv.36.1.105>, 2010. 995
- Wong, M. M. F., Fung, J. C. H., Ching, J., Yeung, P. P. S., Tse, J. W. P., Ren, C., Wang, R., and Cai, M.: Evaluation of uWRF performance and modeling guidance based on WUDAPT and NUDAPT UCP datasets for Hong Kong, *Urban Climate*, 28, 100 460, <https://doi.org/10.1016/j.uclim.2019.100460>, 2019.
- Wouters, H., Demuzere, M., Blahak, U., Fortuniak, K., Maiheu, B., Camps, J., Tielemans, D., and van Lipzig, N. P.: Efficient urban canopy parametrization for atmospheric modelling: description and application with the COSMO-CLM model (version 5.0\_clm6) for a Belgian Summer, *Geoscientific Model Development*, 9, 3027–3054, <https://doi.org/10.5194/gmd-9-3027-2016>, 2016. 1000
- Wu, Y., Sharifi, A., Yang, P., Borjigin, H., Murakami, D., and Yamagata, Y.: Mapping building carbon emissions within local climate zones in Shanghai, *Energy Procedia*, 152, 815–822, <https://doi.org/10.1016/j.egypro.2018.09.195>, 2018.
- Xu, C., Hystad, P., Chen, R., Van Den Hoek, J., Hutchinson, R. A., Hankey, S., and Kennedy, R.: Application of training data affects success in broad-scale local climate zone mapping, *International Journal of Applied Earth Observation and Geoinformation*, 103, 102 482, 1005 <https://doi.org/10.1016/j.jag.2021.102482>, 2021.
- Yamazaki, D., Ikeshima, D., Tawatari, R., Yamaguchi, T., O’Loughlin, F., Neal, J. C., Sampson, C. C., Kanae, S., and Bates, P. D.: A high-accuracy map of global terrain elevations, *Geophysical Research Letters*, 44, 5844–5853, <https://doi.org/10.1002/2017GL072874>, 2017.
- Yang, X., Yao, L., Jin, T., Peng, L. L., Jiang, Z., Hu, Z., and Ye, Y.: Assessing the thermal behavior of different local climate zones in the Nanjing metropolis, China, *Building and Environment*, 137, 171–184, <https://doi.org/10.1016/j.buildenv.2018.04.009>, 2018. 1010
- Yang, X., Peng, L. L., Jiang, Z., Chen, Y., Yao, L., He, Y., and Xu, T.: Impact of urban heat island on energy demand in buildings: Local climate zones in Nanjing, *Applied Energy*, 260, 114 279, <https://doi.org/10.1016/j.apenergy.2019.114279>, 2020.
- Yokoya, N., Ghamisi, P., Xia, J., Sukhanov, S., Heremans, R., Tankoyeu, I., Bechtel, B., Le Saux, B., Moser, G., and Tuia, D.: Open Data for Global Multimodal Land Use Classification: Outcome of the 2017 IEEE GRSS Data Fusion Contest, *IEEE Journal of Selected Topics in Applied Earth Observations and Remote Sensing*, 11, 1363–1377, <https://doi.org/10.1109/JSTARS.2018.2799698>, 2018. 1015
- Yoo, C., Lee, Y., Cho, D., Im, J., and Han, D.: Improving local climate zone classification using incomplete building data and sentinel 2 images based on convolutional neural networks, *Remote Sensing*, 12, 1–22, <https://doi.org/10.3390/rs12213552>, 2020.
- Zhang, X., Liu, L., Wu, C., Chen, X., Gao, Y., Xie, S., and Zhang, B.: Development of a global 30 m impervious surface map using multisource and multitemporal remote sensing datasets with the Google Earth Engine platform, *Earth System Science Data*, 12, 1625–1020 1648, <https://doi.org/10.5194/essd-12-1625-2020>, 2020a.



- Zhang, Y., Kong, D., Gan, R., Chiew, F. H., Mcvigar, T. R., Zhang, Q., and Yang, Y.: Coupled estimation of 500m and 8-day resolution global evapotranspiration and gross primary production in 2002–2017, *Remote Sensing of Environment*, 222, 165–182, <https://doi.org/S003442571830590X>, 2019.
- Zhang, Y., Zhang, J., Zhang, X., Zhou, D., and Gu, Z.: Analyzing the Characteristics of UHI (Urban Heat Island) in Summer Daytime Based on Observations on 50 Sites in 11 LCZ (Local Climate Zone) Types in Xi’an, China, *Sustainability*, 13, 83, <https://doi.org/10.3390/su13010083>, 2020b.
- Zhao, C., Weng, Q., and Hersperger, A. M.: Characterizing the 3-D urban morphology transformation to understand urban-form dynamics: A case study of Austin, Texas, USA, *Landscape and Urban Planning*, 203, 103 881, <https://doi.org/10.1016/j.landurbplan.2020.103881>, 2020a.
- Zhao, L., Oleson, K., Bou-Zeid, E., Krayenhoff, E. S., Bray, A., Zhu, Q., Zheng, Z., Chen, C., and Oppenheimer, M.: Global multi-model projections of local urban climates, *Nature Climate Change*, <https://doi.org/10.1038/s41558-020-00958-8>, 2021.
- Zhao, M., Cheng, C., Zhou, Y., Li, X., Shen, S., and Song, C.: A global dataset of annual urban extents (1992–2020) from harmonized nighttime lights, *Earth System Science Data*, 14, 517–534, <https://doi.org/10.5194/essd-14-517-2022>, 2022.
- Zhao, Z., Shen, L., Li, L., Wang, H., and He, B.-J.: Local Climate Zone Classification Scheme Can Also Indicate Local-Scale Urban Ventilation Performance: An Evidence-Based Study, *Atmosphere*, 11, 776, <https://doi.org/10.3390/atmos11080776>, 2020b.
- Zhou, Y., Smith, S. J., Zhao, K., Imhoff, M., Thomson, A., Bond-Lamberty, B., Asrar, G. R., Zhang, X., He, C., and Elvidge, C. D.: A global map of urban extent from nightlights, *Environmental Research Letters*, 10, 054 011, <https://doi.org/10.1088/1748-9326/10/5/054011>, 2015.
- Zhu, X. X., Qiu, C., Hu, J., Shi, Y., Wang, Y., Schmitt, M., and Taubenböck, H.: The urban morphology on our planet – Global perspectives from space, *Remote Sensing of Environment*, 269, 112 794, <https://doi.org/10.1016/j.rse.2021.112794>, 2022.
- Zhu, Z., Zhou, Y., Seto, K. C., Stokes, E. C., Deng, C., Pickett, S. T., and Taubenböck, H.: Understanding an urbanizing planet: Strategic directions for remote sensing, *Remote Sensing of Environment*, 228, 164–182, <https://doi.org/10.1016/j.rse.2019.04.020>, 2019.
- Zhuo, L., Zheng, J., Zhang, X., Li, J., and Liu, L.: An improved method of night-time light saturation reduction based on EVI, *International Journal of Remote Sensing*, 36, 4114–4130, <https://doi.org/10.1080/01431161.2015.1073861>, 2015.
- Zhuo, L., Shi, Q., Tao, H., Zheng, J., and Li, Q.: An improved temporal mixture analysis unmixing method for estimating impervious surface area based on MODIS and DMSP-OLS data, *ISPRS Journal of Photogrammetry and Remote Sensing*, 142, 64–77, <https://doi.org/10.1016/j.isprsjprs.2018.05.016>, 2018.
- Zonato, A., Martilli, A., Di Sabatino, S., Zardi, D., and Giovannini, L.: Evaluating the performance of a novel WUDAPT averaging technique to define urban morphology with mesoscale models, *Urban Climate*, 31, 100 584, <https://doi.org/10.1016/j.uclim.2020.100584>, 2020.
- Zong, L., Liu, S., Yang, Y., Ren, G., Yu, M., Zhang, Y., and Li, Y.: Synergistic Influence of Local Climate Zones and Wind Speeds on the Urban Heat Island and Heat Waves in the Megacity of Beijing, China, *Frontiers in Earth Science*, 9, <https://doi.org/10.3389/feart.2021.673786>, 2021.



# Appendix

## Appendix A: WUDAPT's digitisation guidelines

1055 In order to guide a user in the digitisation of LCZ training area polygons, a set of digitisation guidelines are provided on the WUDAPT webpage ([www.wudapt.org/digitize-training-areas/](http://www.wudapt.org/digitize-training-areas/)). This information is split in two parts, discussing: 1) how to digitize a LCZ polygon using Google Earth and the provided .kml template, and 2) good practice guidelines for digitisation (Figure A1).



Property	Examples	
<p><b>Size</b></p> <p>Think at the local scale. Individual buildings do not constitute an LCZ. Look for large homogenous areas that are at a minimum 200 m wide at the narrowest point. Use Google Earth's measurement tool to ensure the area is large enough.</p>		
<p><b>Shape</b></p> <p>Avoid complex shapes, as this can lead to mixed spectral information. Simple block shapes however will maximize the homogeneity of the spectral information and the number of available satellite pixels available within the shape.</p>		
<p><b>Homogeneity</b></p> <p>If you digitize a training area, the surface characteristics should be similar. In case of doubt, better to digitize different training areas that are homogeneous than one area that is too heterogeneous.</p>		
<p><b>Borders   Distance</b></p> <p>Try to keep a minimum distance to other LCZs when classifying. If polygons from different classes are too close to each other, the classifier will receive mixed spectral signals which will affect the quality of the classification.</p> <p>Similarly, do not digitize your training area too close to other land cover(s). Also, avoid precise digitization along road or river segments, features that are often too narrow.</p>		
<p><b>Persistence   Seasonality</b></p> <p>Avoid construction sites, as they are likely to change LCZ type during a short period of time.</p>		
<p>The surface characteristics of some LCZ types may depend on the seasonality. Agricultural areas (LCZ D, crops) are a typical example, where land cover may flip from bare soil to cultivated land throughout the year. Use the Google Earth's time slider to explore seasonality.</p>		
<p>Keep in mind tidal or seasonal waters. Depending on the time of day or season of the year, shorelines or river beds might be dry or contain water.</p>		
<p><b>Spatial Distribution</b></p> <p>Distribute training areas over the entire region of interest, as the same LCZs might differ in their appearance and spectral properties for different parts of your region of interest.</p>		

Figure A1. Good practice guidelines for digitising LCZ training area polygons (© Google Earth 2020).



## Appendix B: GLCM texture and NANTLI input features

1060 To date, very few studies tested the added value of texture features (derived from the Gray-Level Co-occurrence Matrix, GLCM) in the LCZ classification procedure. Forget et al. (2018) found that combining features computed from both Sentinel-1 VV and VH backscatter polarisations consistently led to better LCZ classification performances in twelve Sub-Saharan African urban areas, even though the introduction of textures computed from different spatial scales did not improve the classification performances. Along the same lines, Hu et al. (2018) found that Sentinel-1 dual-Pol SAR data (including texture features) can  
1065 contribute to the classification of transcontinental cities into several LCZ classes. Also Brousse et al. (2020a) successfully used Sentinel-1 GLCM texture features with an 11 by 11 kernel window size to map nine Sub-Saharan African urban areas, in order to better capture the heterogeneities of built up surfaces.

Since Sentinel-1 backscatter information is already available in the input feature space, and inspired by the findings of Hay  
1070 Chung et al. (2021), PALSAR (Phased Array type L-band Synthetic Aperture Radar, Shimada et al. (2014)) backscattering information was added. Yet not the pure HH and HV backscatter information as in Hay Chung et al. (2021), but rather the GLCM texture features derived from them (Haralick et al., 1973; Connors et al., 1984; Chen et al., 2021a), as follows:

1. a median 2017-2019 PALSAR composite is created for both the HH and HV polarisation backscattering coefficients;
2. for each polarisation, the eighteen GLCM texture features are derived, with a 2 by 2 and 4 by 4 kernel window, corre-  
1075 sponding to a 50 and 100 m spatial resolution, respectively;
3. only the contrast, dissimilarity, inertia, sum average, and cluster shade texture measures are retained, as the remaining textures indicated little added value in the LCZ mapping (not shown).

In addition, also the Visible Infrared Imaging Radiometer Suite (VIIRS) Day/Night Band (DNB), provided by Mills et al. (2013), was used as follows:

- 1080 1. a median 2017-2019 composite is created from the monthly VIIRS Stray Light Corrected Nighttime Day/Night Band Composites (NTL);
2. this median NTL image is smoothed with a convolution filter using a radius of 300 meter;
3. afterwards, the smoothed NTL image as normalised (hereafter referred to as  $NTL_{norm}$ );
4. NANTLI is calculated, a Normalized Difference Vegetation Index (NDVI) adjusted NTL Index, according to Eq. B1.

$$1085 \quad NANTLI = \frac{1 + (NTL_{norm} - NDVI)}{1 - (NTL_{norm} - NDVI)} \times NTL \quad (B1)$$



Note that NANTLI is analogous to EANTLI (Zhuo et al., 2015), yet uses the Landsat 8 NDVI input feature available from Demuzere et al. (2021b) instead of EVI (Enhanced Vegetation Index), introduced to mitigate both saturation problems and blooming effects of VIIRS data (Zhuo et al., 2018; Zhang et al., 2020a).

The added value of these features are evaluated by mapping 45 cities (three cities per urban ecoregion, characterised by large TA samples with a large number of different LCZ classes) into LCZs, following the procedure of the LCZ Generator Demuzere et al. (2021b), but each time using a different set of earth observation input features. This results in four experiments:

- GEN: the default 33 input features available from the LCZ Generator;
- GEN+NANTLI: GEN and NANTLI
- GEN+NANTLI+P2: GEN, NANTLI and the PALSAR texture features derived with kernel size 2 by 2
- GEN+NANTLI+P4: GEN, NANTLI and the PALSAR texture features derived with kernel size 4 by 4.

Results are evaluated in terms of the overall accuracy metrics (OAs) described in Section 2.4. Figure B1(A) displays the OAs for the GEN experiment for each individual city sorted by urban ecoregion (ER 1 - 15). Figures B1(B), B1(C) and B1(D) indicate the change in OAs for GEN+NANTLI, GEN+NANTLI+P2, and GEN+NANTLI+P4 respectively, compared to GEN. Adding NANTLI increases the average OAs between 0.3 and 2%, with individual city values ranging between -1 and 5.8% (for Constantine - ER12 and Cologne - ER2, respectively). Adding PALSAR texture features further increases the average OAs between 0.8 and 3.2% (GEN+NANTLI+P2, Fig. B1(C)) and 0.9 and 3.8% (GEN+NANTLI+P4, Fig. B1(D)). Here, individual city values range between -0.3 (Itanagar, ER14) and 7.8% (Rosario, ER4) for GEN+NANTLI+P2 and -0.9 (Havana, ER6) and 13.8% (Rosaria) for GEN+NANTLI+P4. As such, the VIIRS-based NANTLI input feature together with the PALSAR-BASED GLCM texture features, using a 4 by 4 kernel size, are selected as additional earth observation for the LCZ mapping procedure.

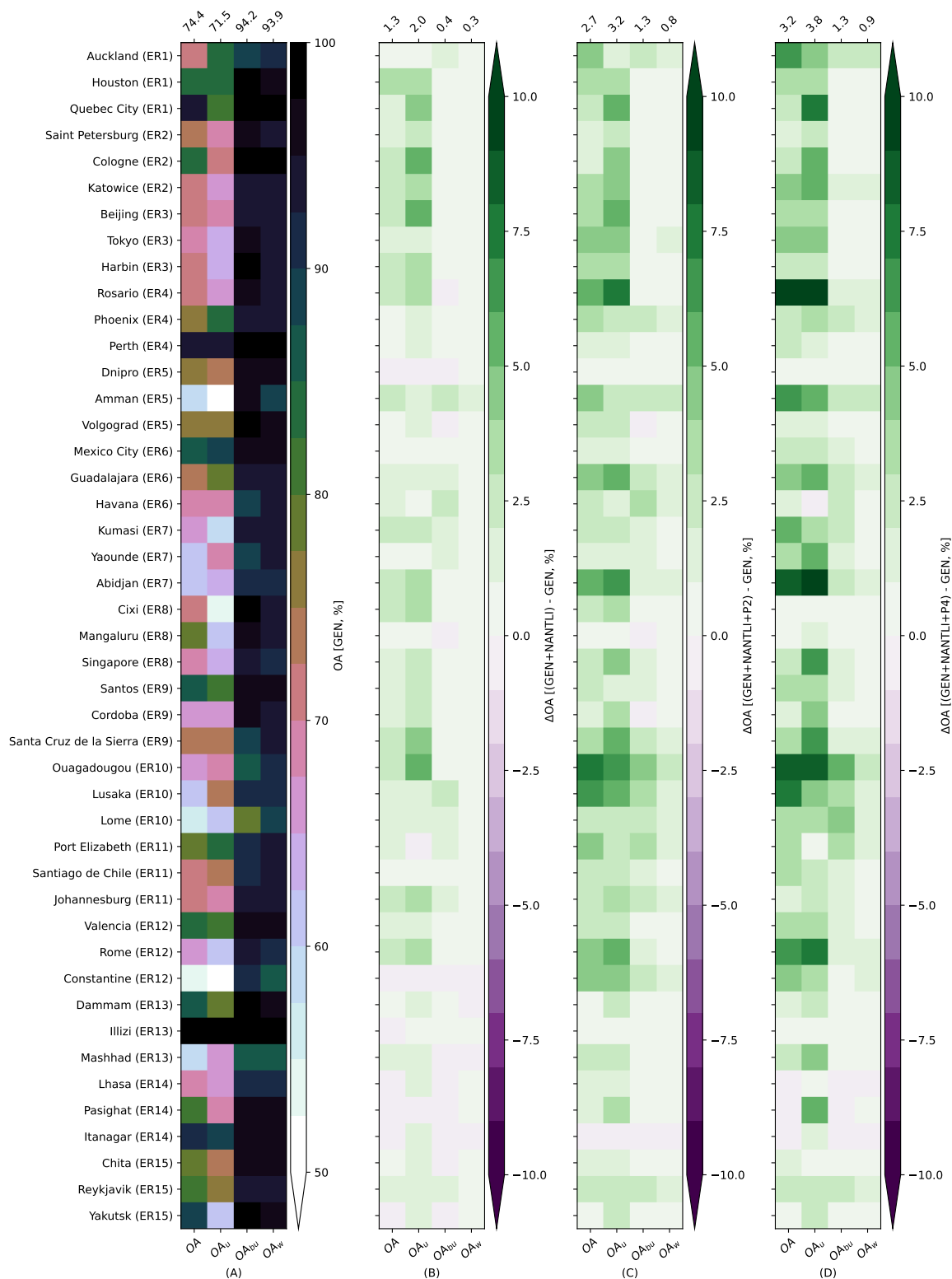


**Figure B1.** Overall accuracies for the various input feature experiments (A) and absolute overall accuracies for all cities for GEN (A), and differences in overall accuracies for experiments GEN+NANTLI (B), GEN+NANTLI+P2 (C), and GEN+NANTLI+P4 (D), compared to GEN. Numbers on the top x-axis indicate the average overall accuracy (change) across all cities. ER refers to urban ecoregion.



### Appendix C: Selected functional urban areas for thematic benchmark

1110 Functional urban areas (FUAs), as defined by the Organisation for Economic Co-operation and Development (OECD) and the European Union, are sets of contiguous local (administrative) units composed of a city and its surrounding, less densely populated local units that are part of the city's labour market (commuting zone). As such, these units not only offer the opportunity to evaluate more densely built city centres, yet also their sparsely built or natural neighbouring landscapes. The 10 most populated FUAs per urban ecoregion used in the thematic benchmark are depicted in Fig. C1.

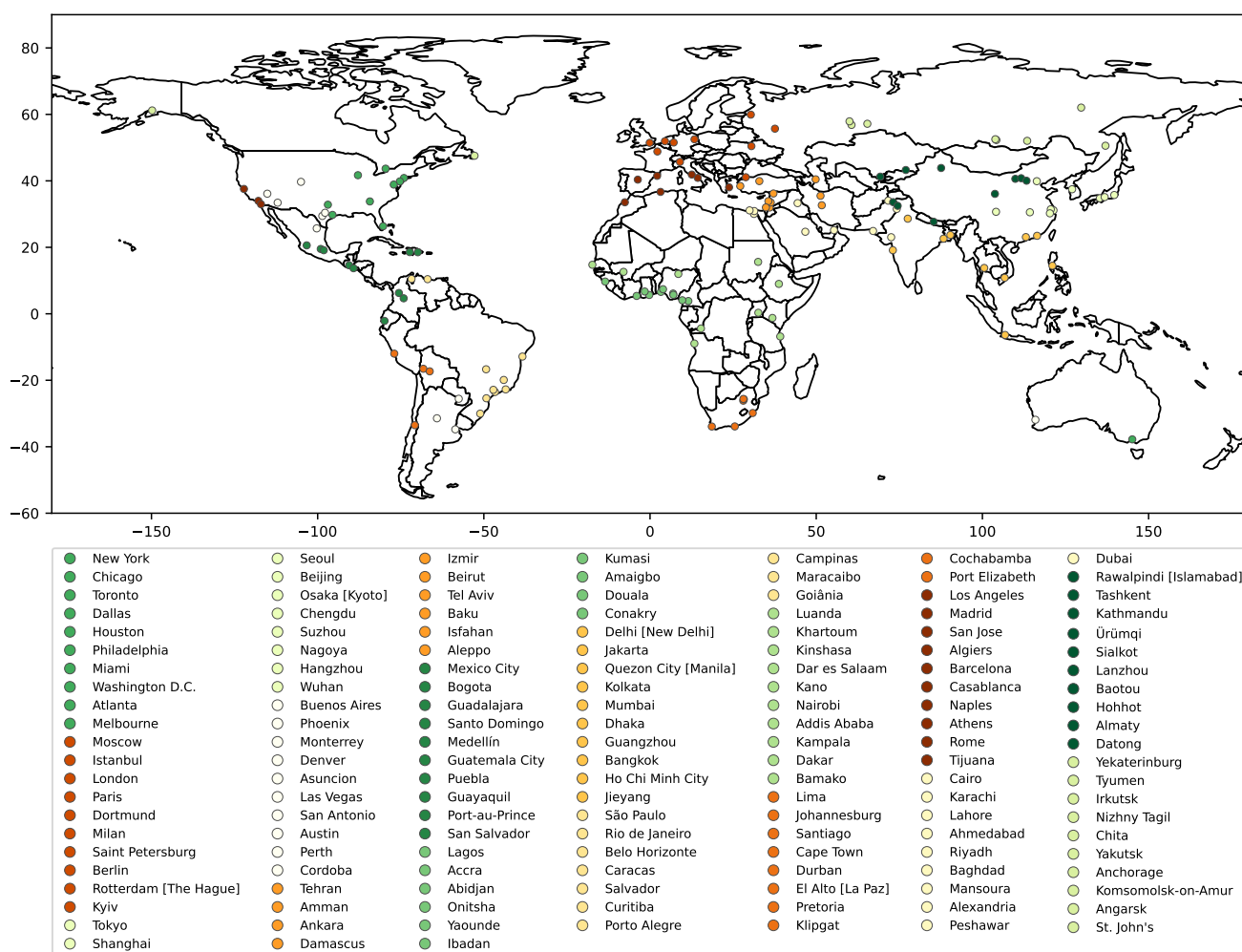


**Figure C1.** Spatial distribution of the 10 most populated functional urban areas per urban ecoregion. Note that ER colors are adopted from Schneider et al. (2010).



## Appendix D: GHS-S2Net versus EEA

1115 Corbane et al. (2021) illustrated that there is a strong relationship between the output probabilities  $p_g$  GHS-S2Net and observed building densities, suggesting that the model outputs can be used as proxy for impervious surface fractions. As an additional benchmark, we evaluate the GHS-S2Net built-up probabilities for the thirty largest (in surface area) European FUAs (Paris, London, Dortmund, Katowice, Oslo, Madrid, Budapest, Warsaw, Berlin, Lyon, Copenhagen, Milan, Frankfurt am Main, Toulouse, Cologne, Hamburg, Vienna, Helsinki, Leeds, Rotterdam, Prague, Belfast, Liège, Rome, Nantes, Gothenburg, Munich, Krakow, Zurich, and Istanbul) against two products from the European Environmental Agency (EEA):

1. the 100 m Copernicus High Resolution Imperviousness Density (IMD) layer for 2018 (European Environment Agency, 2018a), a thematic product that indicates the total sealing density ( $\lambda_T$ ), ranging from 0-100%,
2. the 100 m Share of Built-up (SBU) layer for 2018 (European Environment Agency, 2018b), an aggregated version of the 10 m Impervious Built-up map that indicates the building surface fraction ( $\lambda_B$ ), ranging from 0-100%

1125 In line with Bechtel et al. (2019a), all data layers are resampled to a common 1 km grid. Afterwards, EEA's IMD ( $\lambda_T$ ) and SBU ( $\lambda_B$ ) land-only pixels are regressed against the GHS-S2Net built-up probabilities for all thirty European FUAs (see Figure D1 as an illustration), and the corresponding coefficients of determination ( $R^2$ ) and slopes are reported for  $\lambda_T$  and  $\lambda_B$  separately (Figure D2). Most  $R^2$  values exceed 0.9 for both  $\lambda_T$  and  $\lambda_B$ , confirming that GHS-S2net is able to explain most of the observed EEA impervious surface fractions. On average, the slopes of the regression between the built-up probabilities of GHS-S2Net and EEA's IMD and SBU products are 0.6 and 0.7 respectively. These results confirm the findings of Corbane et al. (2021) that the GHS-S2net built-up probabilities can serve as a proxy for  $\lambda_B$ .

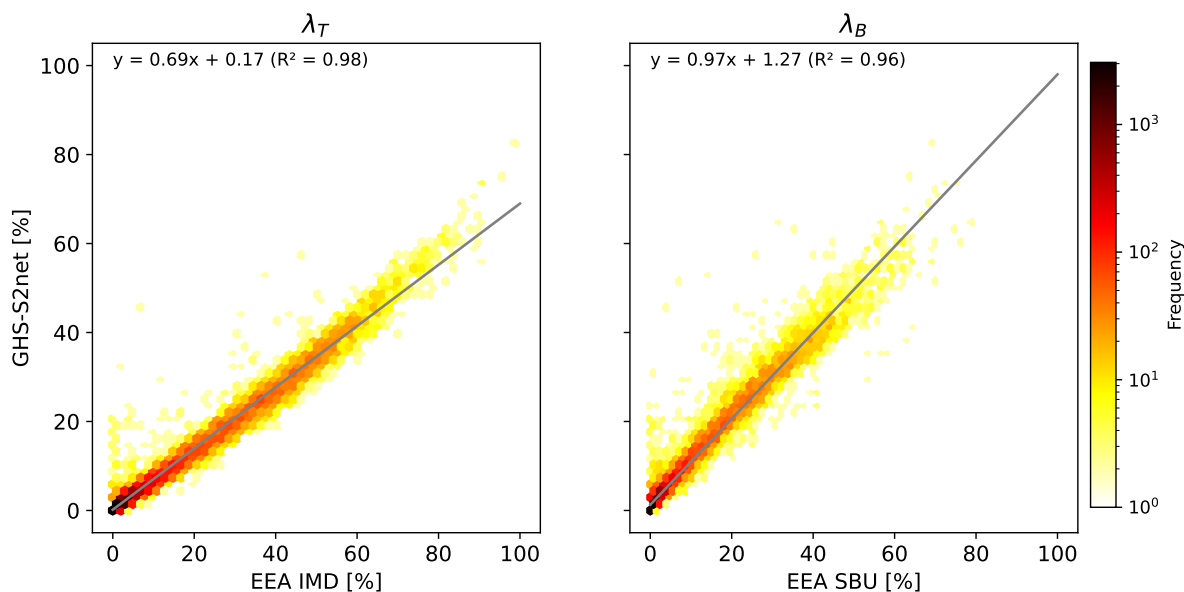


**Figure D1.** Hexbin illustration of the EEA Imperviousness Density (IMD, reflecting  $\lambda_T$ ) and Share of Built-up (SBU, reflecting  $\lambda_B$ ) against GHS-S2Net built-up probabilities for the European Functional Urban Area (FUA) of Dortmund (Germany). Linear regression equations and  $R^2$  values are provided for both  $\lambda_T$  (left panel) and  $\lambda_B$  (right panel). The logarithmic colorbar represents the number of pixels in each imperviousness bin.

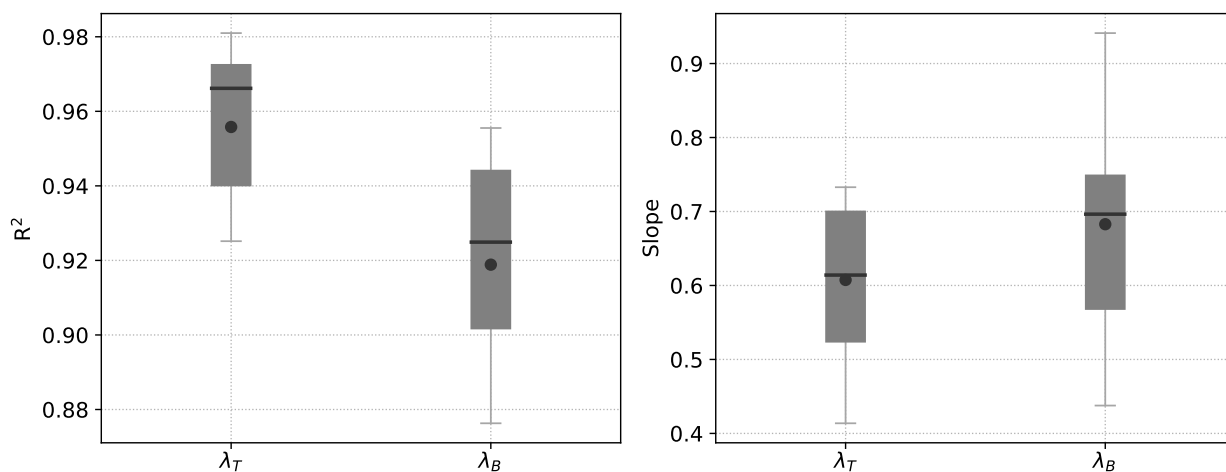


**Figure D2.** Distribution of  $R^2$  values and slopes for the regressions between between GHS-S2Net and EEA's IMD ( $\lambda_T$ ) and SBU ( $\lambda_B$ ) datasets, for the thirty selected European FUA boundaries. Grey boxes and whiskers span the 25–75 and 5–95 percentiles respectively. The means and medians are indicated by the black dots and lines respectively.



### Appendix E: Final number training area polygons per LCZ class

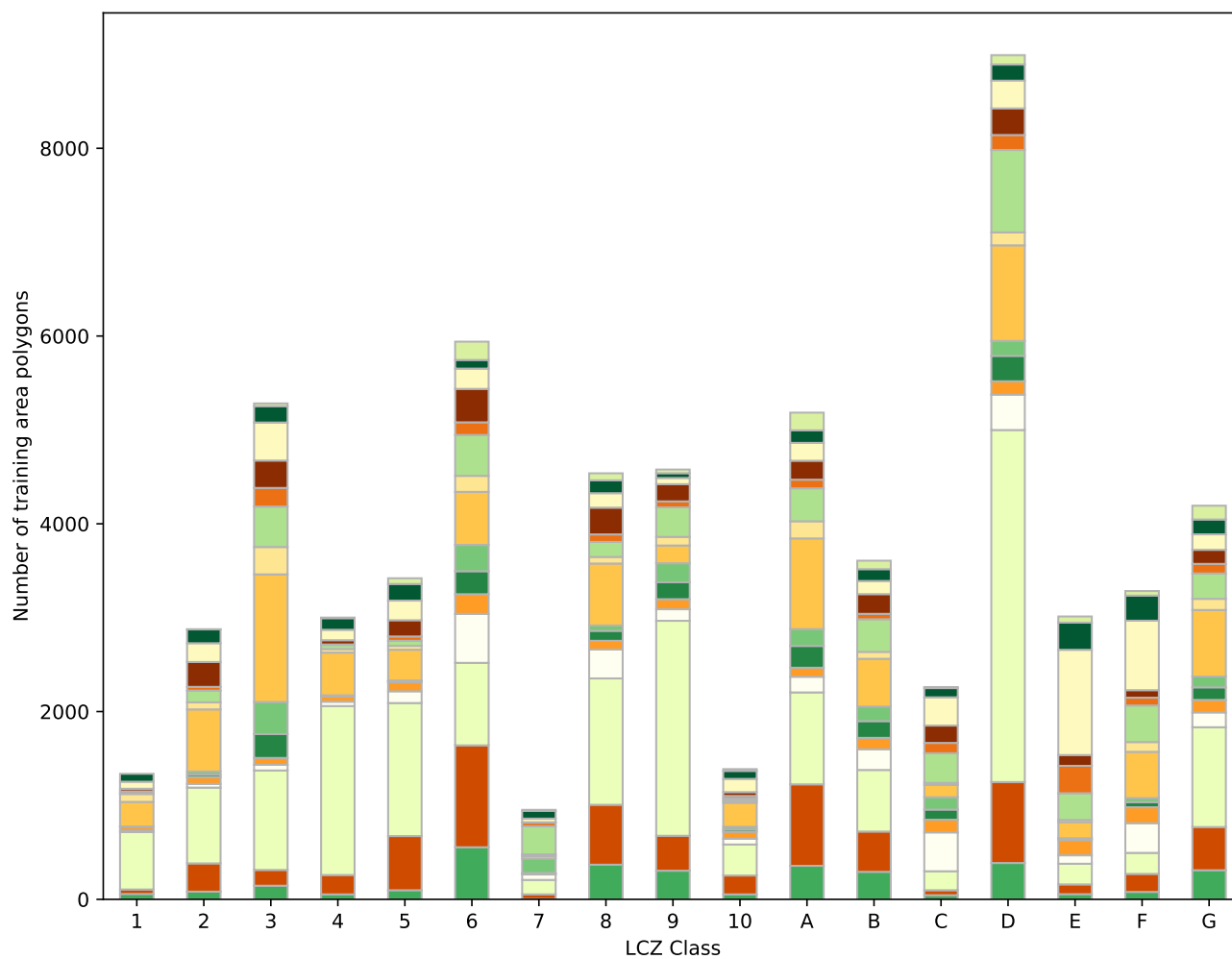


**Figure E1.** Number of training area polygons per LCZ class and ER (colors as in Fig. 3).



### Appendix F: Final input features

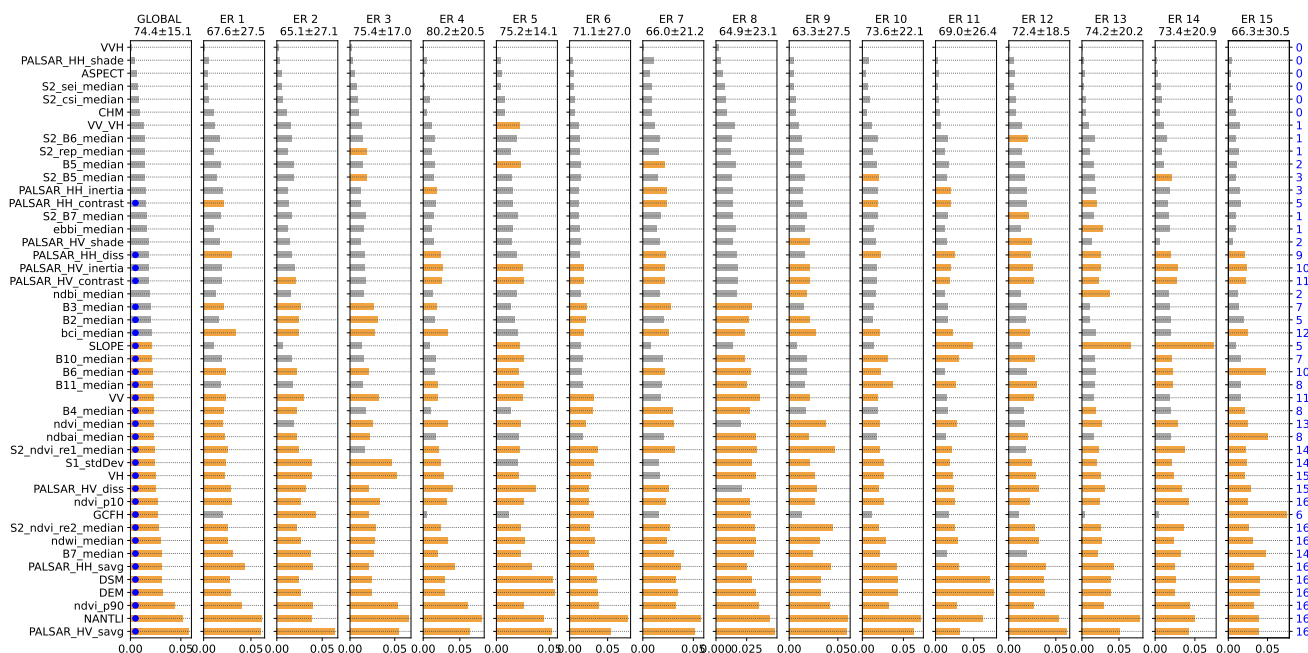


**Figure F1.** Feature importance ranking for the globe and per urban ecoregion (ER). Bars in bright orange depict the input features (per spatial unit) that belong to the top 50% of most important variables. Numbers on top depict the overall accuracy  $\pm$  the standard deviation (%). Blue numbers on the right-hand side describe how often an input feature belongs to the top half of most important features. Features with a value  $\geq 5$  are used in pathway 2 to create the global LCZ map and are indicated by the blue dot in the global panel on the left. These features are described in more the Table F1.



**Table F1.** Final set of input features used in the global LCZ mapping process. The information is structured by sensor, with the input feature names referring to the abbreviations used in the feature importance ranking shown in Fig. F1.

Sensor	Input feature	Description
PALSAR	HH_contrast	Contrast GCLM texture parameter from the HH polarisation backscatter
	HH_dist	Dissimilarity GCLM texture parameter from the HH polarisation backscatter
	HH_savg	Sum average GCLM texture parameter from the HH polarisation backscatter
	HV_contrast	Contrast GCLM texture parameter from the HV polarisation backscatter
	HV_diss	Dissimilarity GCLM texture parameter from the HV polarisation backscatter
	HV_intertia	Inertia GCLM texture parameter from the HV polarisation backscatter
	HV_savg	Sum average GCLM texture parameter from the HV polarisation backscatter
Landsat 8	B2_median	Band 2 (blue) surface reflection median composite
	B3_median	Band 3 (green) surface reflection median composite
	B4_median	Band 4 (red) surface reflection median composite
	B7_median	Band 7 (shortwave infrared 2) surface reflection median composite
	B10_median	Band 10 (brightness temperature) median composite
	B11_median	Band 11 (brightness temperature) median composite
	bci_median	Biophysical Composition Index median composite
	ndbi_median	Normalized Difference Built Index median composite
	ndbai_median	Normalized Difference BAreness Index median composite
	ndvi_p10	10th percentile of the Normalized Difference Vegetation Index composite
	ndvi_median	Normalized Difference Vegetation Index median composite
	ndvi_p90	90th percentile of the Normalized Difference Vegetation Index composite
	ndwi_median	Normalized Difference Water Index median composite
Sentinel-1	VV	Single co-polarization, vertical transmit/vertical receive median composite
	VH	Single co-polarization, horizontal transmit/horizontal receive median composite
	S1_StdDev	Standard deviation of VV and VH combined
Sentinel-2	S2_ndvi_re1_median	Normalized Difference Vegetation Index Red Edge 1 median composite
	S2_ndvi_re2_median	Normalized Difference Vegetation Index Red Edge 2 median composite
Other	DEM	High accuracy global DEM at 3 arc second resolution from MERIT (Multi-Error-Removed Improved-Terrain Digital Elevation Model), version 1.0.3
	DSM	Global digital surface model (DSM) dataset with a horizontal resolution of approximately 30 meters from ALOS World 3D, version 3.2
	SLOPE	Slope derived from the MERIT DEM
	GCFH	Global forest canopy height data
VIIRS	NANTLI	Normalized Difference Vegetation Index adjusted Night-time Light Index, based on Landsat's NDVI and VIIRS Day/Night Band



### Appendix G: Traditional accuracy assessment

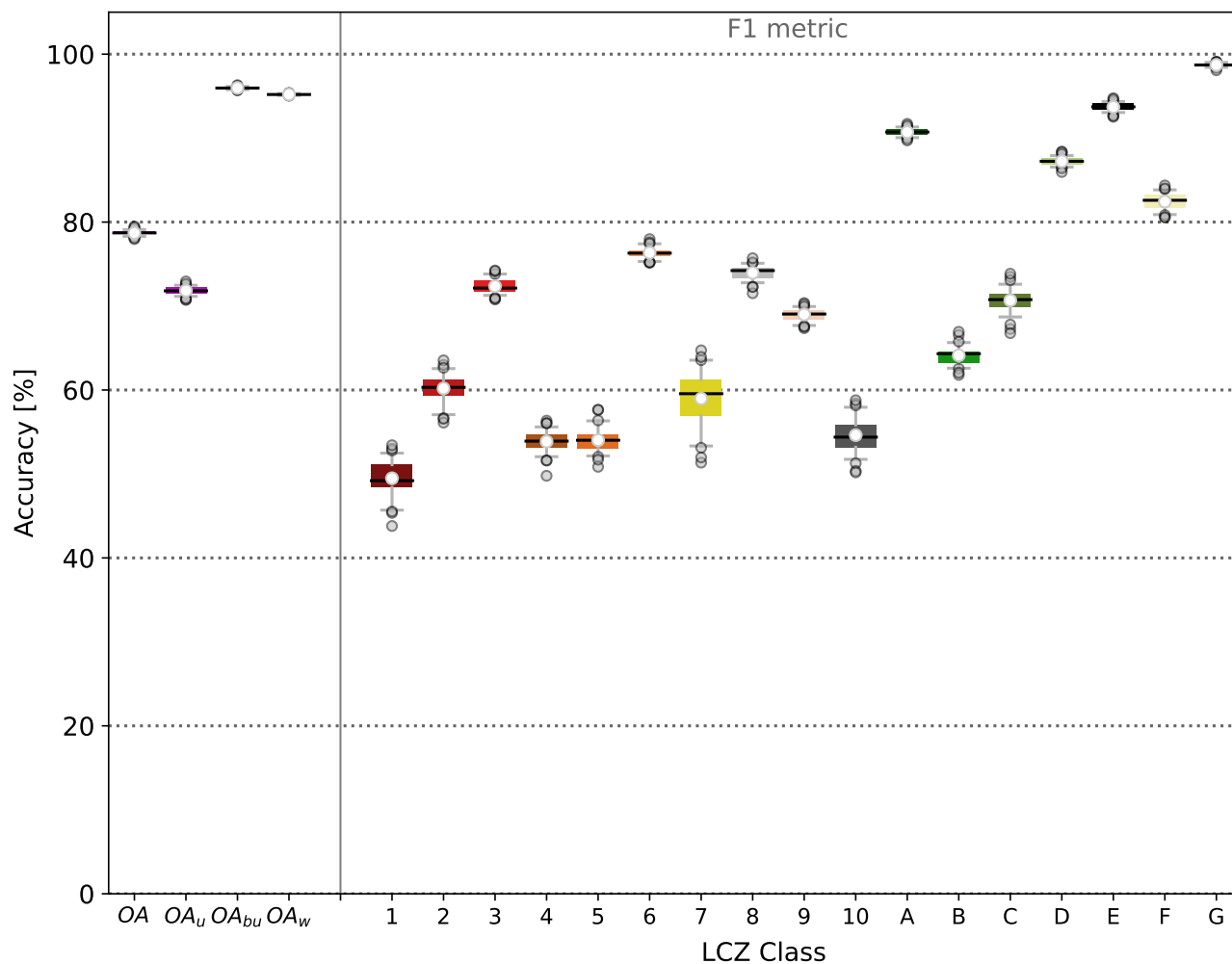


**Figure G1.** Overall and class-wise F1 accuracies for the global random forest LCZ models. Coloured boxes and grey whiskers span the 25-75 and 5-95 percentiles respectively. The means and medians are indicated by the white dots and black lines respectively.



1135 Appendix H: Thematic benchmark results per urban ecoregion

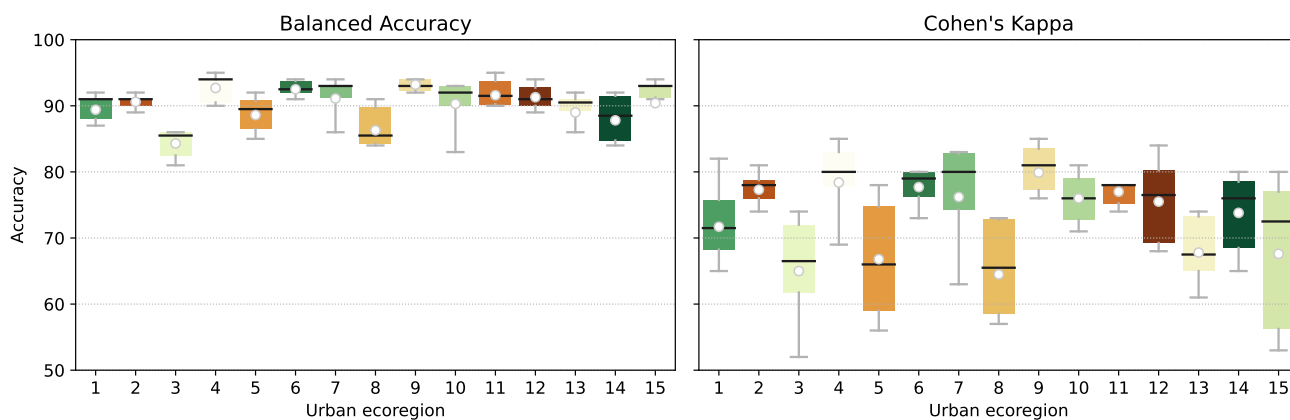


**Figure H1.** Balanced accuracy (left panel) and Cohen's Kappa (right panel) for the 150 global LCZ FUA regions in terms of built-up land, stratified by urban ecoregion (colours as in Fig. 3). Boxes and grey whiskers span the 25-75 and 5-95 percentiles respectively. The means and medians are indicated by the white dots and black lines respectively.

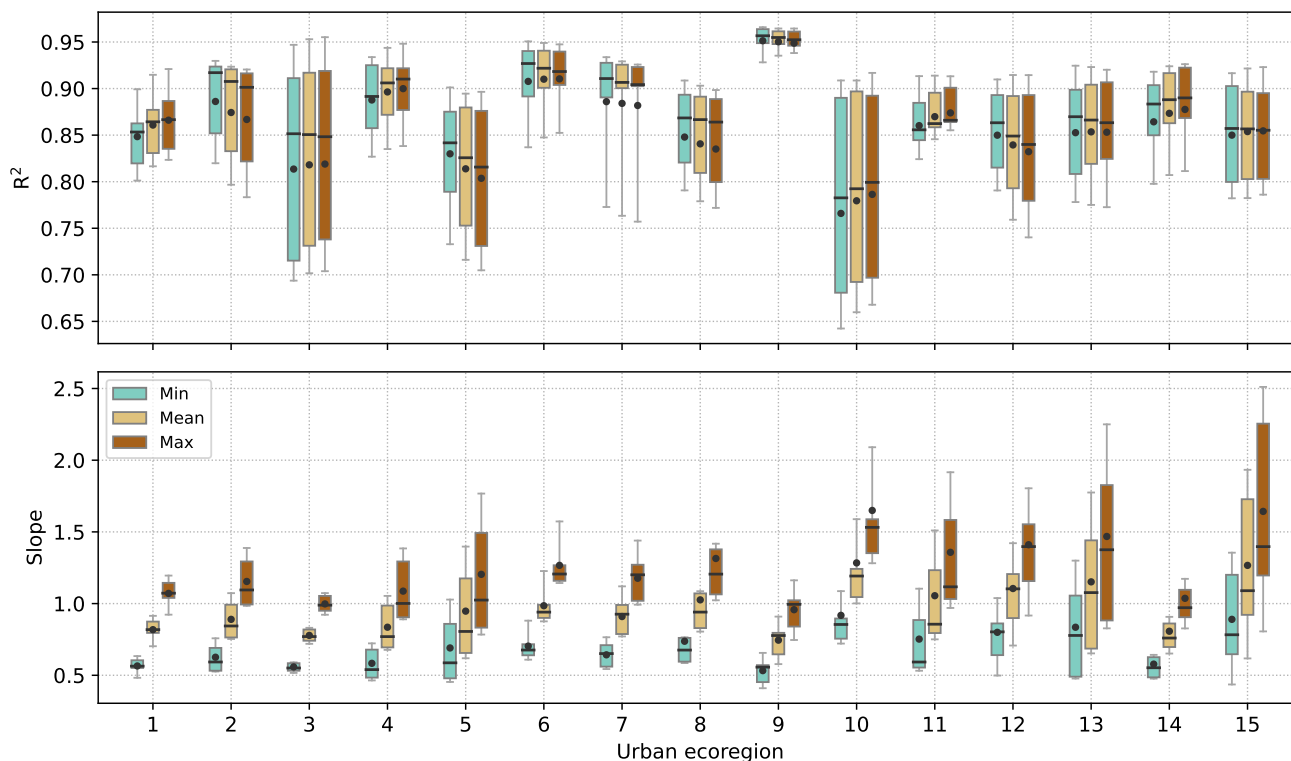


**Figure H2.** Coefficients of determination ( $R^2$ ) and slopes resulting from the regression between the reference dataset for  $\lambda_B$  and the corresponding universal LCZ-based values from Stewart and Oke (2012), using minimum, mean and maximum values (colours), for all FUAs stratified per ecoregion. Coloured boxes and grey whiskers span the 25–75 and 5–95 percentiles respectively. The means and medians are indicated by the black dots and lines respectively.

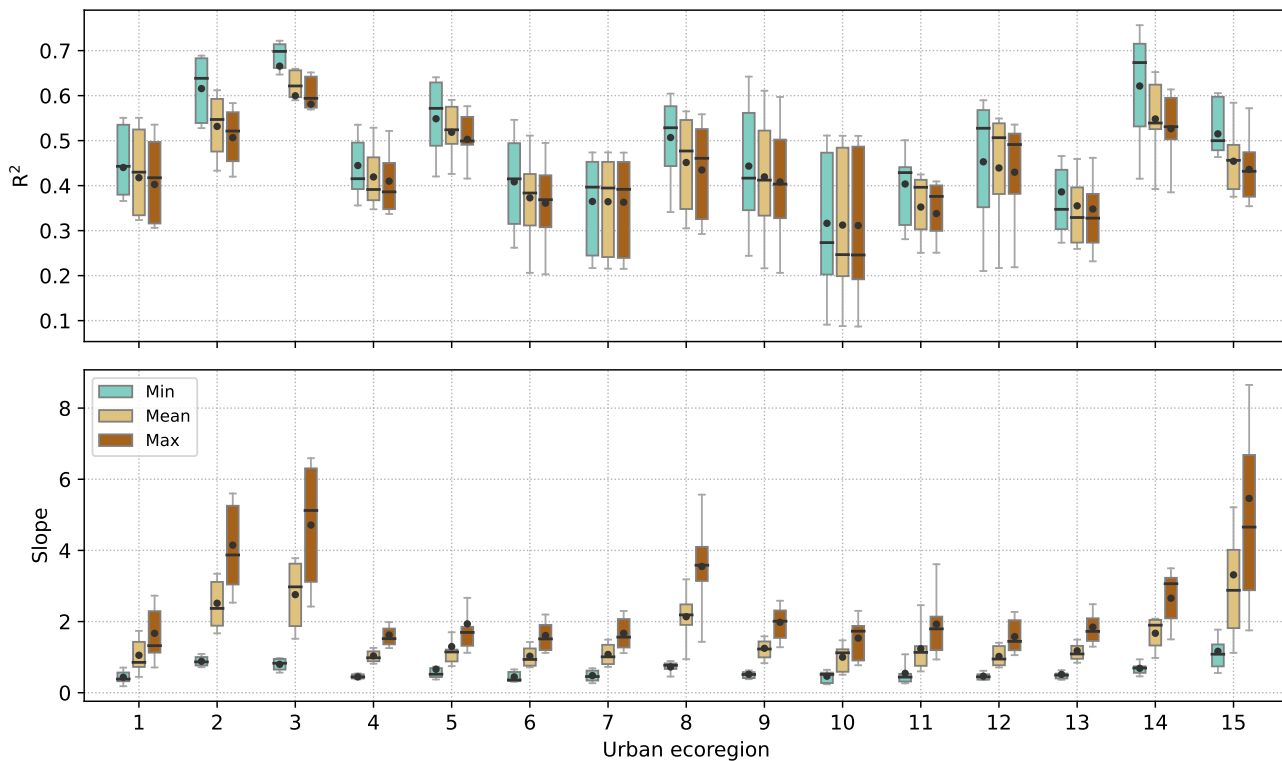


**Figure H3.** As Fig. H2 but for building height  $H$ .

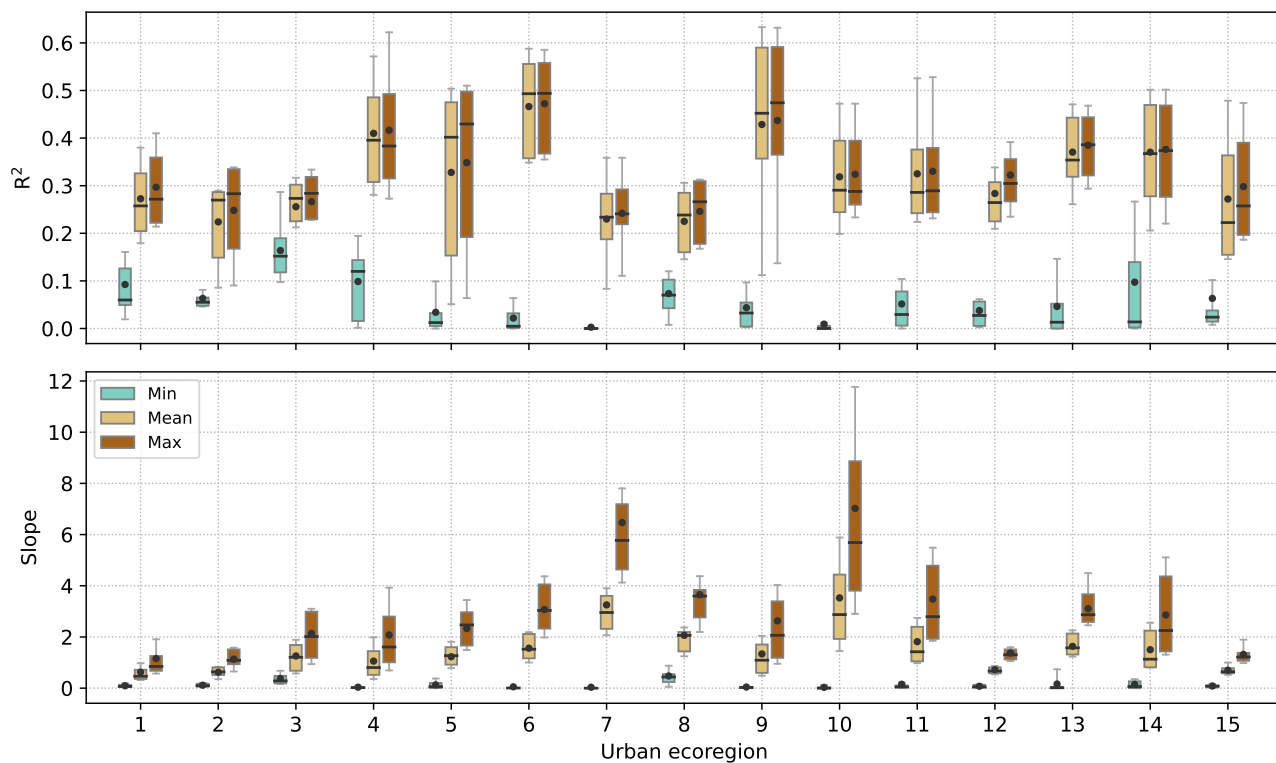


**Figure H4.** As Fig. H2 but for the anthropogenic heat flux *AHF*.